

MOLECULAR BEAM STUDY
OF
POLYATOMIC FREE RADICAL REACTIONS

by

David Lee McFadden
A.B., Occidental College
(1967)

SUBMITTED IN PARTIAL FULFILLMENT OF THE
REQUIREMENTS FOR THE DEGREE OF
DOCTOR OF PHILOSOPHY

at the
MASSACHUSETTS INSTITUTE OF TECHNOLOGY

September, 1972

Signature of Author

Certified by
Thesis Supervisor

Accepted by
Chairman, Departmental Committee
on Graduate Students



This thesis has been examined by:

Professor Carl W. Garland
Chairman of Thesis Committee

Professor James L. Kinsey

Professor John Ross

To Martha and My Parents

MOLECULAR BEAM STUDY OF POLYATOMIC

FREE RADICAL REACTIONS

by

David Lee McFadden

Submitted to the Department of Chemistry on September 1,
1972, in Partial Fulfillment of the Requirements for the
Degree of Doctor of Philosophy

ABSTRACT

A versatile crossed molecular beams apparatus with a "universal" mass spectrometer detector has been designed and constructed. Doubly differentially pumped beams cross at 90° . The angular differential cross section is measured in the plane of the two beams by the rotatable detector which scans an angular range of 130° . There are a total of seven differentially pumped chambers.

A beam source of polyatomic free radicals has been developed which has produced beams of methyl and ethyl radicals of sufficient intensity to carry out reactive scattering experiments.

The product alkyl halide angular distributions from the reactions: $\text{CH}_3 + \text{Cl}_2$, Br_2 , I_2 , ICl and $\text{C}_2\text{H}_5 + \text{Br}_2$, have been measured at thermal energies. Without exception the reaction products peak backward in the center of mass coordinate system with respect to the incoming radical. Trends in the angular distributions are very similar to trends observed in the reactions of D atoms with the same halogens (MCD 72).

Thesis Supervisor

John Ross

Frederick G. Keyes Professor of Chemistry

ACKNOWLEDGEMENTS

I am indebted to Professor John Ross for his guidance and encouragement throughout the course of this work. I am fortunate in having been able both to draw from his far-ranging scientific experience and knowledge and to enjoy his valuable and rewarding friendship.

I gratefully acknowledge the valuable collaboration of my colleagues, Drs. Ron Gentry, Ed McCullough, and Ferenc Kalos in this work. I am particularly indebted to Dr. Ron Gentry for his design of the apparatus and supervisor over its construction.

I have benefited from the stimulating atmosphere of a seminar initiated by Professor J. L. Kinsey and contributed to by the groups of Professors I. Amdur, J. W. Dubrin, J. L. Kinsey, and J. Ross.

The construction of the apparatus was made possible by the excellent facilities and assistance provided by the M.I.T. electronics and machine shops.

I am grateful to Dr. Ed McCullough for his critical reading of the manuscript, to Mr. Mark Chen and Mr. Kwei-Rhu Chien for their assistance in preparing the appendices, and to Ms. Ann Rowbotham for typing the final copy.

TABLE OF CONTENTS

	Page
List of Figures and Tables	8
Introduction	9
Part I CROSSED MOLECULAR BEAMS APPARATUS WITH MASS SPECTROMETER	
DETECTOR	10
A. Introduction to Non-Alkali Beam Experiments	11
B. Apparatus Design Criteria	13
C. General Construction of Apparatus	16
D. Vacuum System	26
1. Static Background	27
2. Dynamic Background	28
3. Vacuum System Details	32
a) Source Chambers	32
b) Main Chamber	34
c) Detector Chambers	36
E. Detector	38
1. Electron Bombardment Ionizer	38
2. Einzel Lens	46
3. Spherical Lens	46
4. Quadrupole Mass Filter	49
5. Final Focusing and Accelerating Lenses	51
6. Ion Counting System	51
a) Channeltron Electron Multiplier	51
b) Pulse Counting Electronics	53
F. Beam Modulation System	55
1. Rotary Chopper	55
2. Diode Signal Amplifier	55

	Page
3. Delay and Gate Generator	58
4. Scaler Gate - Timer/Scaler Synchronizer	61
5. Relay Beam Flag and Chopper	64
 Part II	
MOLECULAR BEAM STUDY OF POLYATOMIC FREE RADICAL REACTIONS . .	68
A. Introduction	69
B. Halogen Molecule Beam Source	70
C. Alkyl Radical Beam Source	77
D. Experimental Procedures	82
E. Measurements	87
F. Features of the Angular Distributions	94
G. Total Reaction Cross Sections	100
H. Discussion	102
 APPENDICES	
A. Currently Available Mechanical Drawings	112
B. Suppliers of Commercial Items	117

FIGURES AND TABLES

<u>FIGURES</u>	Page
1. Horizontal Cross Sectional Drawing of Apparatus.	17
2. Vertical Cross Sectional Drawing of Apparatus.	19
3. Mass Spectrum of Static Background.	29
4. Block Diagram of "Universal" Detector.	39
5. Cross Sectional Drawing of Electron Bombardment Ionizer.	41
6. Schematic Diagram of: Photodiode Signal Amplifier, Delay and Gate Generator, and Synchronizer.	56
7. Timing Diagram of Delay and Gate Generator.	59
8. Timing Diagram of Scaler Gate-Timer/Scaler Synchronizer.	62
9. a) Relay Beam Flag and Chopper Circuit. b) Timing Diagram for Relay Chopper.	65
10. Pyrolysis Source for Alkyl Radicals.	80
11. Laboratory Angular Distributions of Alkyl Halide Reaction Products.	88

TABLES

I. Halogen Molecule Nozzle Beam Source Operating Conditions.	72
II. Representative Experimental Results from the Peaks of the Angular Distribution Measurements.	90
III. Results of lab \rightarrow c.m. Transformation Assuming a Nominal Newton Diagram.	97

Introduction

The ability to observe single collisions between reactive species in molecular beam experiments has existed for nearly two decades. For many years the field of Molecular Beams remained separate and distinct, with little interplay between it and other areas of more "traditional" chemistry. This isolation was due in large part to the limited scope of chemical systems amenable to study by surface ionization detection techniques. With the development of the "universal" mass spectrometer detector came the potential for extending molecular beam research to areas of inorganic and organic chemistry previously unexplored by these techniques.

In this spirit we set out to demonstrate the possibility of studying organic free radical reactions in molecular beams. The first successful angular distribution measurements of polyatomic free radical reactions are presented in Part II of this thesis.

In order to carry out these studies we designed and constructed a versatile crossed beams apparatus with a rotatable mass spectrometer detector. In the broadest terms it is capable of measuring the angular differential scattering cross section of any binary collision process of chemical interest. There is no fundamental limitation which dictates the range of chemical species or energies to be studied. A description of this apparatus with emphasis on the design criteria for studying neutral-neutral reactions at thermal energy is presented in Part I.

Part I

CROSSED MOLECULAR BEAMS APPARATUS
WITH MASS SPECTROMETER DETECTOR

A. Introduction to Non-Alkali Beam Experiments

The work described here commenced in the fall of 1967. At that time molecular beam studies of chemical reactions yielding neutral products were limited to atom-molecule reactions involving a surface ionizable species. The "universal" detector had not as yet been successfully adapted to the study of reactions in crossed beams, though work on this problem was in progress in several laboratories. Reactive signals had been seen from the reactions of $D + H_2$, $H + D_2$, and $D + Br_2$, but it was impossible to elucidate any detail in these experiments (DAT 63, FIT 63, FIT 65, DAT 67).

In addition to the successes of the "supermachine" described here, the work in other laboratories has also come to fruition. Two apparatuses are described in detail in the literature (LEE 69, BIC 70), and a number of studies of non-alkali atom-molecule reactions have been published (LEE 69b, LEE 68, BEC 68, CRO 69, CRO 70, GED 70, GRO 70, SCH 70, MCD 72). On the more negative side however, only halogen atom and deuterium atom reactions have been reported. An appreciation of the relative difficulty of non-alkali experiments is necessary in order to understand why only a limited number of systems have been studied and why at least three machines built for "universal" detection of reaction products have not yet performed successfully.

In contrast to the complexity of "supermachines", the apparatuses employed in the early alkali experiments were relatively simple. The two beam sources and the detector were typically located in a single chamber. The products were detected by surface ionization which is specific for alkali metals and their salts. Therefore only the partial

pressure of the alkali species had to be low, and liquid nitrogen cryo-pumping sufficed in maintaining adequately low background signals.

Differential pumping of the sources or detector was not necessary. This enabled all components to be placed close to the intersection volume, thus minimizing $1/R^2$ intensity losses. Add to this the unit efficiency of hot wire detection and the large cross sections of most of the early alkali reactions (on the order of 100 \AA^2). In retrospect it is not difficult to see why it was possible to do experiments using relatively weak, nearly effusive beams and analogue current measurements of the scattered products.

The increased difficulty of non-alkali experiments is due to several factors. The maximum efficiency of electron bombardment detection is $\sim 0.1\%$. Furthermore, in order for the apparatus to be generally useful, signals from reactions with total cross sections of order 1 \AA^2 must be measurable. From these rough figures, if all other factors remain constant, the signal from a typical non-alkali reaction would be a factor of 10^5 smaller than that from an alkali reaction. This does not include the increased problem of interfering background at the mass of the reaction products. As mentioned above the background in alkali experiments is not particularly troublesome because of the low vapor pressure of the alkali metals and salts at liquid nitrogen temperature. Many non-alkali reactants and products do not have this favorable property. To make things worse, the background partial pressure at the mass of interest must be reduced to $\sim 10^{-14}$ torr because of the relatively small signals expected. Therefore different and more drastic pumping schemes are required. In addition to the ultrahigh vacuum requirements, the system must be able to handle heavier gas loads as well, since more intense

beams are necessary to make up for the typically smaller cross sections. In every respect the problems faced in designing a non-alkali "super-machine" are of greater magnitude and demand more sophisticated technological solutions than those encountered in the early alkali work.

Presented in the sections which follow is a description of an apparatus whose design has successfully overcome these difficulties for at least one class of non-alkali reactions never before studied by molecular beam techniques (see Part II).

B. Apparatus Design Criteria

The design of any experimental apparatus is based on an analysis of signal to noise considerations. The true signal in crossed beams reactive scattering experiments comes from the formation of product molecules in the intersection volume as a result of collisions between reactant beam molecules. Product molecules so produced which scatter directly into the detector are measured as a function of laboratory scattering angle. Present at all times is an interfering background signal which comes from the detection of product molecules (or molecules of the same mass as product molecules) formed in some other way. Residual atmospheric gases, collisions of beam molecules with the ambient background gas, and molecules formed in the intersection volume but indirectly scattered into the detector after repeated wall collisions, are common sources of background. In principle at least, the true signal can be separated from the background signal by means of beam modulation. This simply consists of interrupting or chopping one beam so that reactant molecules in that beam arrive at the intersection region in bunches with a given frequency.

The true signal will arrive at the detector with the same frequency, while the background signal is a constant D.C. signal. Two detector channels are synchronized with the beam chopper so that one channel (Signal Channel) is active only when true signal is arriving at the detector. The other channel (Background Channel) is only active between bunches of true signal. The signal channel thus records true signal plus the D.C. background signal, and the background channel records only the background signal. The difference between the two channels is the true signal. The complications introduced by a modulated contribution to the background are discussed below.

The limiting source of noise in these experiments is the statistical variations in the true signal and in the background (LEE 69). Following the arguments given in (LEE 69) and (KIN 72) we find that during a time interval t , the total number of events counted at the detector is $N_1 = \epsilon(S+B)t$ in the signal channel and $N_2 = \epsilon Bt$ in the background channel. S and B are the concentrations of molecules contributing to the signal and background, respectively, and ϵ the counting rate produced by a unit concentration where ϵ is an efficiency factor for the entire detection train. A statistical fluctuation of one standard deviation is $N^{1/2}$ where $N = N_1 + N_2$, the total number of counts accumulated by the detector in time t . Since the signal accumulates linearly with time and the statistical noise increases as $t^{1/2}$, by counting sufficiently long at one angular setting the signal to noise ratio R can be made arbitrarily large. Practically speaking t must be kept on the order of 10^3 seconds to allow the entire angular distribution to be measured within a reasonable length of time. The counting time required to achieve a desired

$R = \frac{\epsilon St}{(N_1 + N_2)^{1/2}}$ is given by $t = \frac{R^2(S+2B)}{\epsilon S^2}$. Under usual conditions $S \ll B$ and $t \propto \frac{B}{S^2}$, which emphasizes the need to maximize both S and S/B . If we take $R^2/t \equiv P$ as a measure of the performance of the apparatus, and ask what the fractional improvement in P is for a fractional change in the variables S , B , and ϵ we find:

$$\delta P_{\epsilon} \equiv \frac{\partial P/P}{\partial \epsilon/\epsilon} = \left(\frac{\partial \ln P}{\partial \ln \epsilon} \right)_{S,B} = 1$$

$$\delta P_S \equiv \left(\frac{\partial \ln P}{\partial \ln S} \right)_{B,\epsilon} = 1 + \frac{2B}{S+2B} \sim 2$$

$$\delta P_B \equiv - \left(\frac{\partial \ln P}{\partial \ln B} \right)_{S,\epsilon} = \frac{2B}{S+2B} \sim 1$$

Therefore increasing the signal is roughly twice as effective in increasing the performance of the apparatus as is increasing the detector efficiency or reducing the background. Nevertheless, the design must focus on all three factors simultaneously; for experience has shown that neglecting to optimize the design for any one of these factors has disastrous results. Every feature in the design of the vacuum system, detection system, and the beam sources was incorporated either to maximize the signal, maximize the detection efficiency, or minimize the background.

It should of course be mentioned that the variables ϵ , S , and B are not necessarily independent, as implied in the previous discussion. For example, factors which increase S may also increase B , and the inter-relationship of these variables may depend on the particular chemical system which is studied. Optimization of a particular variable implies a maximization of R and not necessarily a maximum or minimum value of

the variable itself.

C. General Construction of Apparatus

Figures 1 and 2 depict the basic features of the apparatus. The central unit of construction is a large box (main chamber) with inside dimensions 26" x 22¹/₂" x 11¹/₂". The box has a rotatable lid 25" in diameter. Additional chambers are mounted on each vertical face of the main chamber. An 8" diameter port is located in each face. The concept of a central chamber on which all other components are supported allows for maximum versatility in adapting the apparatus to the specific requirements of each experiment. In Fig. 1 four chambers can be seen mounted on the outside walls of the main chamber, while two chambers are located inside. 5.4" diameter ports are bored in the bottom of the main chamber for differential pumping of the two chambers located inside the main chamber. A 14" diameter pumping port is also bored in the bottom of the main chamber. One entire side of the main chamber is removable if less hindered access than through one of the 8" ports is necessary. Two additional ports are bored in the main chamber and five in the rotatable lid for general purposes such as electrical or liquid nitrogen feedthroughs. The location of sixteen tapped holes on the top corners of the main chamber serve to mount a step ladder, the drive gear assembly for the lid, and brackets for removing the lid from the chamber. An electric chain hoist which travels on an I-beam suspended above the apparatus is used for lifting the lid and other heavy pieces into place.

The rotatable lid carries the mass spectrometer detector and its pumping system. The lid is rotated manually with a 20:1 reduction gear

Figure 1

Horizontal Cross Sectional View of Apparatus

- a. Main chamber
- b. Source pumping chamber 1
- c. Removable bulkhead separating source chambers 1 and 2
- d. Source pumping chamber 2
- e. Liquid helium cryopump chamber
- f. Detector buffer chamber
- g. Detector chamber
- h. Beam source mounting flange
- r. Electron bombardment ionizer
- DP. Oil Diffusion pump
- TiSP. Titanium sublimation pump
- L He. Liquid helium cryopump

The scanning range of the detector should be 130° instead of 120° .

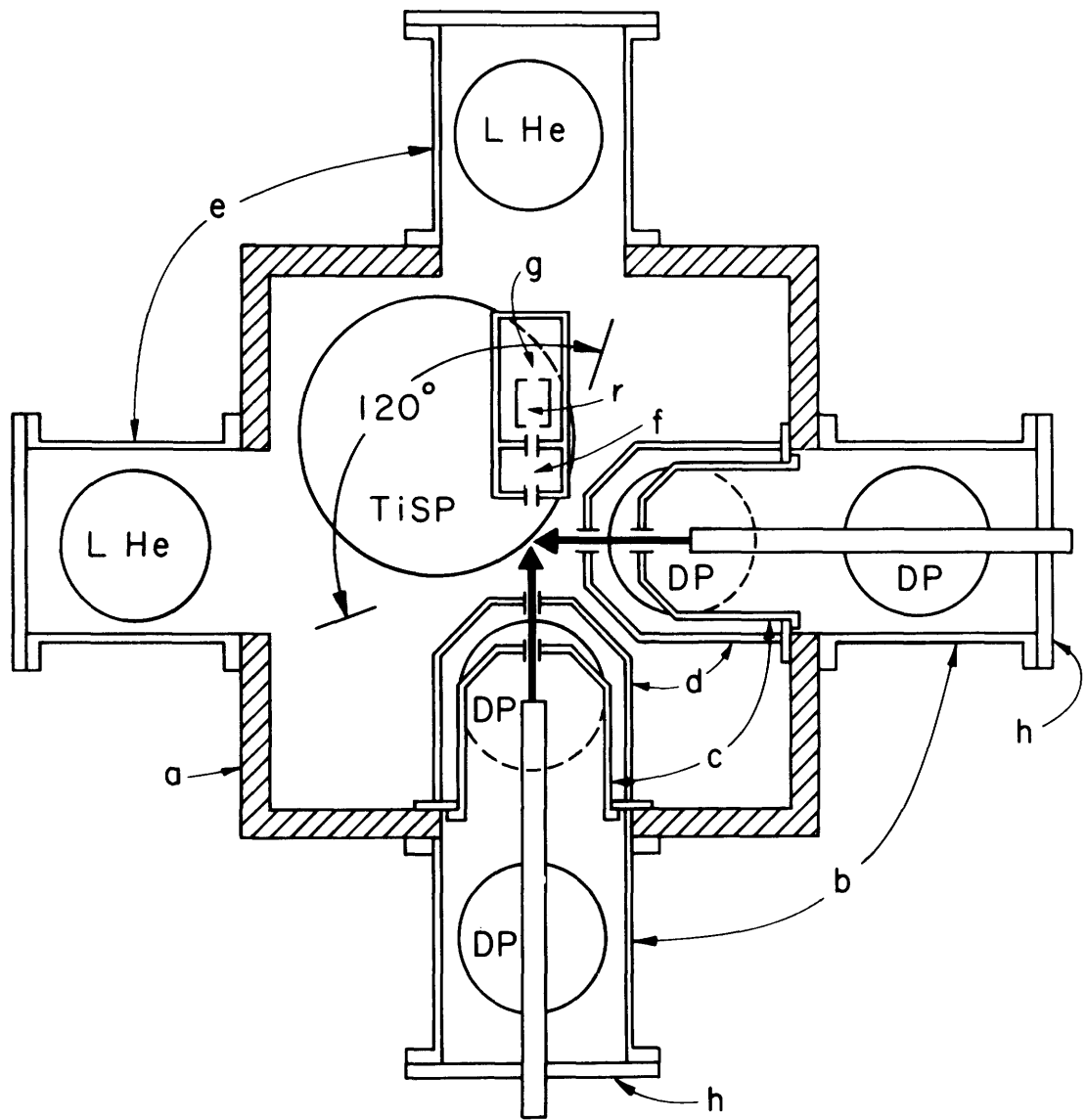
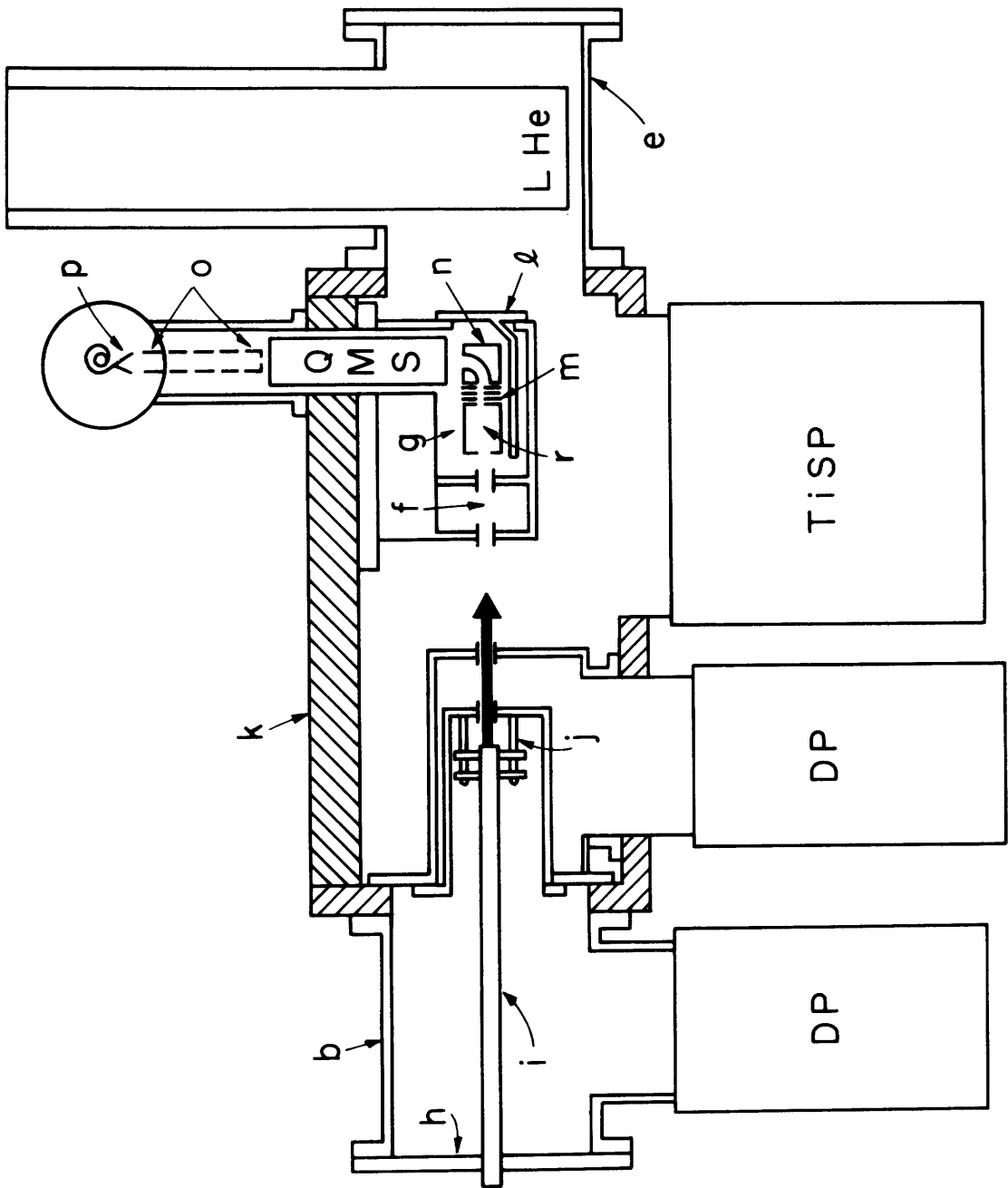


Figure 2

Vertical Cross Sectional View of Apparatus

- b. Source pumping chamber 1
- e. Liquid helium cryopump chamber
- f. Detector buffer chamber
- g. Detector chamber
- h. Beam source mounting flange
- i. Beam source tube
- j. Beam source tube alignment and support pins
- k. Rotatable lid
- l. Detector chamber back flange and mounting bench
- m. 3 element einzel lens
- n. Spherical lens
- o. 5 element high voltage cylindrical lens
- p. Channeltron electron multiplier
- r. Electron bombardment ionizer
- DP. Oil diffusion pump
- TiSP. Titanium sublimation pump
- L He. Liquid helium cryopump
- QMS. Quadrupole mass spectrometer

The detector pumping system, which mounts on the rotatable lid is not shown; neither are the extensive liquid nitrogen cooled cold shields.



drive. It is supported by a circular ball bearing which must withstand the total weight of the lid (~ 300 lbs.) and the pressure difference when the main chamber is evacuated ($\sim 7,000$ lbs.).

The entire apparatus is constructed of type 304 stainless steel. The main advantage of stainless steel over other materials such as brass or aluminum is that it is chemically inert and presents a low outgassing surface to the vacuum. The 300 series was chosen because it is non-magnetic. The most troublesome property of stainless steel is its hardness. Even for a skilled craftsman machining time is roughly a factor of two longer for stainless steel than for brass, aluminum, or other soft metals. (A novel approach in the choice of construction materials which has the advantages of both stainless steel and a softer metal was taken by R. W. Anderson at the University of California, Santa Cruz. His chamber is fabricated from soft steel which is inexpensive and easy to machine. After construction the interior of the chamber was nickel-plated so as to be corrosion resistant.)

The conventional method of joining two pieces of stainless steel is to heliarc weld them. Certain disadvantages accompany this method. Welding introduces strains into the metal which must be relieved by annealing before the final machining is completed. Stress relieving prevents the gradual distortion of surfaces due to such strains. In high vacuum work it is always advisable to weld joints on the inside seam which faces the vacuum. This eliminates the possibility of small trapped volumes which create troublesome virtual leaks. The smaller the piece the more difficult it is to weld inside joints. Finally, heliarc welding is a process which leaves a piece dirty by ultra-high vacuum standards and chemical cleaning is often necessary. In an attempt to eliminate these diffi-

culties hydrogen brazing was used instead of heliarc welding. In one step in the brazing furnace, the pieces are joined, stress relieved, and cleaned. Furthermore, brazing inside joints is no particular problem regardless of the size of the piece. Although this method appeared to have many advantages over heliarc welding, it turned out to be a more time-consuming process. This is due to the long cycle times (~ 12 hours) for brazing and the fact that horizontal and vertical joints cannot be brazed simultaneously.

A simple procedure for precision alignment of the beam sources, the beam collimating apertures, and the detection components has been planned for in the design. The smaller the collimating apertures the more accurate the alignment must be. Although relatively wide beams and large detector apertures are used in the present studies, all apertures are interchangeable and overall tolerances meet the requirements of the smallest of these. In order to facilitate precision alignment of the various components that are mounted on the main chamber, all of its opposite surfaces are parallel, and adjacent surfaces are perpendicular to within $\pm .005$ " overall. The side ports of the main chamber and the rotatable lid are centered on perpendicular lines which come to within $\pm .003$ " of intersecting in the center of the main chamber. Reference lines are inscribed on each vertical face of the main chamber to aid in locating these center lines. The walls of the main chamber and the lid are thick (1.25" and 3" respectively) to insure that atmospheric pressure will not distort the chamber. The main chamber is essentially an optical bench on which every other chamber and component is mounted. However, this only partially solves the alignment problem. Proper alignment refers to the location of the two beam sources, four beam collimating apertures,

two detector apertures, and the detection components. The centers of all these elements must lie in the same horizontal plane within the desired tolerances. Since the apertures are located in the bulkheads separating the various chambers, and the beam sources and detection components are supported by the chambers in which they sit, the problem of positioning these elements becomes a problem in the design of the source chambers, the source differential pumping chambers, and the detection chambers. The original design of these chambers was based on the following notion. If all chambers are precision machined such that the location of the apertures with respect to the mounting surfaces is exact within very close tolerance, then when the various chambers are mounted on the main chamber, which is also precision machined, the alignment of all apertures will be correct without adjustment. Furthermore, if the beam sources and detection components are accurately attached to flanges which can be precisely mounted on their respective chambers, then the alignment of these components is determined. Removal and replacement of the flanges does not disturb the alignment. Without going into the details of how this is carried out, it can be seen that every component built has critical dimensions requiring tolerances held typically to $\pm .005$ ". In principle there is nothing wrong with this reasoning but practical considerations weigh heavily against adopting this design concept. Machining to close tolerances not only takes longer if perfectly executed but also is more subject to irreparable errors which cause additional time to be lost in remachining. When these factors are multiplied by the number of jobs requiring high precision, it is not difficult to see how months of delay were suffered in the construction of the apparatus.

Having experienced these difficulties, when it became necessary to

rebuild the source differential pumping chambers for other reasons, an alternative alignment scheme was adopted. Here the apertures are mounted on small flanges which are screwed to the chamber bulkheads in approximately the correct position. Wide clearance holes in the aperture flanges allow for adjustment. Alignment is accomplished with the aid of a helium-neon laser after the chambers are in place. Since the procedure is required only once, the savings in machining time and cost with this design far outweigh the time saved in alignment with the original design. In fact, a similar alignment procedure was used originally as a final check that all tolerances had been held. Certainly a design is adequate if it insures the success of the experiment. However, the difference between an adequate and an optimum design can make a tremendous difference in time and money. Simple alignment of the beam sources is also accomplished with this design. The first collimating aperture for each beam is located in the bulkhead between the source chamber and the source differential pumping chamber. Two locating pins are placed symmetrically on the flange which holds the aperture. These pins project into the source chamber and serve as support and alignment pins for the beam source tube (see Fig. 2). Therefore alignment of the apertures insures beam source alignment. Originally the beam sources were supported only on the flange at the back of the source chamber; there was no support close to the first collimating aperture. Since the aperture is located approximately 20" from the back flange, alignment was a difficult task. Precision machining was required on the source chambers, the source chamber flanges, and the beam source tubes. Furthermore, since the beam source tubes are usually heated during an experiment, alignment can be

destroyed when non-uniform expansions are magnified over a distance of 20". Supporting the source tube close to the collimating aperture minimizes heating distortions and greatly reduces the number of parts responsible for the alignment of the beam.

The detector chamber design, which has not been modified, follows the original alignment concept. The horizontal plane of the beams is defined by the intersecting center lines of the main chamber side ports. The bottom surface of the rotatable lid is parallel to this plane and located a precise distance above it. The bottom of the lid is a reference point for the location of the detection components and the collimating apertures. The distance from the center of the detector apertures to the face of the flange which attaches to the lid is held to tolerances of $\pm .005$ ". A design similar to that adopted for the beam collimating apertures should be considered if the detector chamber is rebuilt. Alignment (without adjustment) of the detection components is also provided for in the construction of the detector chamber. The electron bombardment ionizer, einzel lens, and spherical lens are mounted on a bench which is attached to a removable flange on the back of the detector chamber (see Fig. 2). This flange is keyed to the cutout in the detector chamber, and the bench is located with respect to the key such that the apertures in the various components lie in the plane of the beams. Therefore the ionizer may be removed and replaced without disturbing the alignment. An alternative design based on being able to adjust the height of the bench would lessen the tolerances on all parts and simplify the construction.

D. Vacuum System

The first requirement of the vacuum system is that the beams must not be attenuated by collisions with the ambient gas particles. This condition is equivalent to demanding that the mean free path be at least comparable to the dimensions of the apparatus. A rule-of-thumb relating the mean free path in air to the pressure is: $\lambda(\text{cm}) = 5/P(\text{microns})$. A pressure of 1×10^{-5} torr corresponds to a mean free path of 5 meters. If this were the only requirement of the vacuum system, the apparatus would consist of one chamber pumped by a high speed oil diffusion pump. However, the need to reduce the background partial pressure of product molecules in the region of the ionizer to a level comparable to the true signal level ($\sim 10^{-14}$ torr) places far more stringent conditions on the design. What are the sources of background? First there is a contribution which I call static background. This is the signal observed at the particular mass of interest when both beams are completely shut off (not just blocked). The partial pressure of air at the mass of the products, outgassing of construction materials, and backstreaming or contamination from certain types of vacuum pumps are common sources of static background. Secondly there is a dynamic contribution to the background signal which results from turning on the beams and introducing reactant molecules into the vacuum system. As reactions occur throughout the apparatus, the steady state concentration of product molecules increases, thus raising the background signal. We are confronted with two distinct problems: How to remove molecules which reside originally in the region of the electron bombardment ionizer and how to keep molecules which are not produced in the beam intersection region from reach-

ing the detector?

D - 1. Static Background

Static background is proportional to the total pressure of gas in the region of the electron bombardment ionizer, where neutral particles are converted to measurable ions. In order to achieve the lowest ultimate pressure in this region the detector is isolated from the rest of the apparatus in its own chamber and pumped continuously. The detector pumping system must provide high pumping speeds at low pressures without contaminating the vacuum. A combination of liquid helium cryopumps and ion pumps meets these requirements. Ion pumps may be operated continuously, have adequate pumping speed for all gases at low pressure, are extremely clean, and capable of attaining vacua in the low 10^{-10} torr range. Liquid helium cryopumps operate during experiments and provide extremely high pumping speeds for all gases except hydrogen and helium. The limit of the attainable vacuum is set by the outgassing of construction materials and sealing gaskets. This calls for a careful cleaning of all parts and the use of low outgassing materials wherever possible. Copper and indium gaskets are used almost exclusively on the detector chamber. Whenever rubber O-rings are used, they are ungreased viton. Insulators are all ceramic. The importance of continuous pumping for the reduction of static background cannot be overemphasized. The detector is sealed from the rest of the apparatus by means of a valve which covers the first detector aperture. This valve is operated from the top of the rotatable lid and opened only when the entire apparatus is under high vacuum. The detector chamber is maintained under

high vacuum with the valve closed, even when the rest of the apparatus is at atmospheric pressure. Continuous pumping gradually degasses the walls of the chamber and other components over a period of weeks, and as this occurs the static background steadily drops. High temperature bake-out accelerates this process. The region surrounding the ionizer is certainly the most critical and is baked-out by continuous operation of the tungsten filament in the ionizer. This filament operates at $\sim 2500^{\circ}\text{K}$ and dissipates ~ 25 watts. A copper shroud immediately surrounding the ionizer is heated by radiation to $\sim 425^{\circ}\text{K}$. During experiments this shroud is cooled to liquid nitrogen temperature giving a bake-out differential temperature of $\sim 350^{\circ}$.

Fig. 3 shows a typical mass spectrum of static background which can be attained using the techniques mentioned here. Above about mass 40 the partial pressure of every mass is sufficiently low to allow the detection of reaction products. However, many reactions which yield products lighter than mass 40 are practically impossible to study by electron bombardment detection because of the large static background.

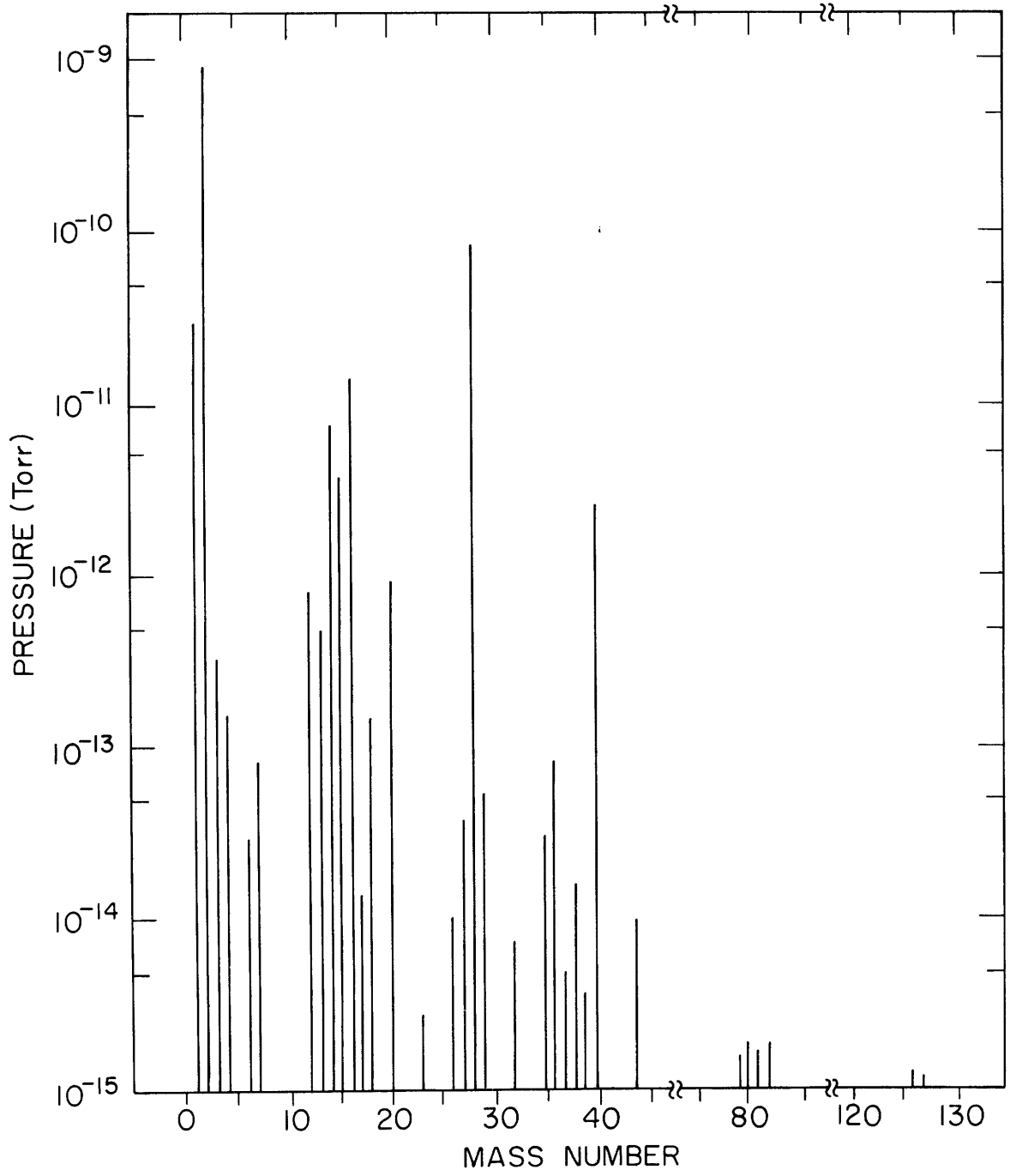
D - 2. Dynamic Background

The vacuum system must be designed such that when the beams are running, the partial pressure of reaction products in the ionizer background gas does not exceed $\sim 10^{-14}$ torr. The background in the ionizer goes up as a result of reactions in the main chamber where the reactants are "mixed". Particles from one beam scatter reactively from ambient background particles of the other reactant. This can be particularly

Figure 3

Mass spectrum of static background

Figure taken from (LEE 69). The background in our detector is similar except at the mass peaks corresponding to halogen atoms and molecules, zinc, and cadmium. Large background levels at these masses gradually built up during the course of the experiments discussed in Part II.



troublesome if the beam being scattered is chopped, for it can produce a modulated background signal. Product molecules created in this way may be directly scattered into the detector if the reactions occur in a volume element subtended by the detector. If formed at some point not directly viewed by the detector they flow effusively into the detector as a result of random wall collisions. In any case the higher the partial pressure of reactants in the main chamber, the higher the product background at the ionizer. Reactive collisions at the walls of the chamber add to the background in the same way. In order to minimize the concentration of reactants in the main chamber, both beam sources are differentially pumped. Most of the gas which flows out of the source tube does not pass through the collimating apertures to become part of the beam. It should be obvious that if the source tube is placed in a separately (or differentially) pumped chamber which connects to the main chamber only through the collimating aperture, then a large fraction of the non-collimated gas will be pumped away and never enter the main chamber. With this arrangement there are two contributions to the background in the main chamber: the beam gas which passes directly from the source tube through the collimating aperture, and the ambient gas in the source pumping chamber which effuses through the collimating apertures. Simple steady state flow equations can be used to calculate the relative magnitudes of these contributions. It can be shown that one differentially pumped chamber makes the two contributions roughly equal. Remember that without differential pumping the non-collimated gas is much greater than the beam gas under typical conditions. Another stage of differential pumping between the source chamber and the main

chamber essentially eliminates the role of effusion from non-collimated background gas in comparison to the flow of beam gas. The background pressure in the main chamber can be further reduced by allowing each beam to pass into yet another differential pumping chamber after traversing the main chamber, but this is seldom necessary and is not incorporated in the present design.

High speed differential pumping of the sources and the main chamber reduces the partial pressure of product molecules within the main chamber to a level still orders of magnitude greater than the true reactive signal reaching the detector. Two stages of differential pumping for the detector are necessary to reduce the effusion of product molecules into the detector to the minimum level set by direct-line flow from the main chamber. The pumping speed for the main chamber and the source chambers must be large to minimize even the direct-line flow. Differential pumping of the detector chambers is accomplished by means of liquid helium cryopumping for the most part.

The problem of dynamic background in neutral-neutral reactive scattering is extraordinary. It does more to complicate the design of the apparatus than any other single factor.

D - 3. Vacuum System Details

a. Source Chambers

The four source differential pumping chambers are each provided with an unbaffled NRC VHS 4 oil diffusion pump. Each pump is rated at a speed of 1200 liters/sec and has a constant pumping speed below 10^{-3} torr. Diffusion pumps are ideally suited to handle the relatively large gas

loads in source chamber applications where typical operating pressures are as high as 10^{-4} torr. Two Welch 1397 mechanical pumps serve as fore pumps. Each diffusion pump can be isolated from its respective chamber by means of an NRC 1283-4 slide valve. The slide valve stem seals are differentially pumped by a Welch model 1402 mechanical pump. The source chambers are designed so that the source nozzle is placed as close as possible to the intersection of the two beams while still preserving two stages of differential pumping. As one can see in Fig. 2 this has the effect of locating the source nozzle and first collimating aperture a considerable distance from the throat of the diffusion pump in source chamber 1. The pumping speed for the heavy gas loads at the nozzle is limited by the conductance of source chamber 1. Similarly the volume between the first and second beam collimating apertures is necessarily small, and the bulkhead between the two source chambers hinders the flow of gas to the diffusion pump in source chamber 2. The pumping speed in the regions of the nozzle and the apertures is considerably less than the rated value of the pumps. One very effective way to increase pumping speed for condensible gases is to use liquid nitrogen cryopumping. Liquid nitrogen cooled copper sheets (nickel-plated to reduce corrosion) are placed close to the source nozzle and apertures, covering as much surface in source chambers 1 and 2 as possible. The conductance to the pumping surface is very large, and sticking coefficients at liquid nitrogen temperature determine the pumping speed. The cold shields are supplied with liquid nitrogen by two gravity-feed dewars (Linde CR-10) mounted atop the #1 source chamber. Stainless steel Swageloks and nickel gasket Cajon high vacuum couplings are used to make liquid nitrogen connections inside the vacuum.

The problem of low conductance is unavoidable because the source nozzle and collimating apertures must be located close together and near the intersection zone. However, the larger the volume of the chambers, the easier it is to provide the highest possible conductance to the pumps from these restricted volumes. In this respect our apparatus is too small. If the main chamber were twice the size it is now, the source pumping chambers could be made in such a way that the removable bulkhead would present much less of an obstruction to the flow of gas. The space within source chamber 1 could also be enlarged considerably. The size of the apparatus should be determined by pumping speed requirements.

All gaskets for source chamber flanges are viton rubber O-rings, making access to the chambers particularly simple. There is no need for gaskets between adjacent source chambers or between source chamber 2 and the main chamber. Far more gas leaks through the apertures connecting these chambers than through the metal to metal seals formed where the chambers are screwed together. The O-ring grooves which are machined on the inside walls of the main chamber for the purpose of vacuum sealing source chamber 2 from the main chamber are unnecessary.

b. Main Chamber

The main chamber is equipped with a combination of liquid helium cryopumps and a titanium sublimation pump. A custom-made Janis liquid helium cryopump is located opposite each beam source (see Figures 1 and 2). They are mounted in T-shaped chambers which attach to the main chamber. The pumps are located so that the beams impact directly on the cryopumps. This produces some of the effect of differentially

pumping the beam after it traverses the main chamber even though an 8" diameter port connects the two chambers. A liquid nitrogen cooled chevron baffle surrounds the liquid helium reservoir to reduce the boil-off rate. A 14" Ultek Boostivac Titanium Sublimation pump is mounted under the main chamber. It has very high pumping speed for many gases at low pressure. Important exceptions are rare gases, light hydrocarbons, and halogens. The combination of sublimation and helium cryopumping provides a total pumping speed in the main chamber in excess of 13,000 liters/sec. Experiments to date have shown that the liquid helium pumping suffices. The titanium pump turns out to be more trouble to operate than it's worth, and plans are being made to replace it with a 10" oil diffusion pump. Originally oil pumps were avoided in the main chamber because it was feared that backstreaming of pump oil would contaminate the detector chamber. However, the vapor pressure of silicone oil (especially Dow Corning 705) is low enough at liquid nitrogen temperature so that this is not a problem. The most pronounced advantages of an oil diffusion pump over the sublimation pump are constant pumping speed and high speed for helium. This last point is essential for running seeded nozzle beams of helium.

A liquid nitrogen cooled cold shield lines the main chamber. It is nickel-plated copper, cooled by conduction, and fed by a 25 liter gravity-feed dewar mounted on the side of the main chamber (Linde CR-25). A Welch model 1397 mechanical pump, baffled by a Granville-Phillips molecular sieve trap, is connected to the main chamber for the purpose of "roughing" the vacuum system down to the micron pressure range. A CVC 2" oil diffusion pump with a Granville-Phillips liquid nitrogen

baffle has also been added below the titanium pump to assist in pumping the system down and to provide pumping speed for rare gases at low pressure. Of course this pump will not be necessary when the titanium pump is replaced by an oil diffusion pump. Gaskets on the main chamber consist of viton rubber O-rings where seals are likely to be broken frequently and copper where ease of access is not crucial. This division is unnecessary. Since the presence of rubber in the main chamber, like that of diffusion pump oil, does not contaminate the detector background, there is no real need for copper gaskets which have several disadvantages. Copper sealing surfaces (knife edges, hemitorroidal surfaces, etc.) are difficult to machine in comparison to O-ring grooves. Many more screws are necessary to compress copper gaskets, and the gaskets are not reusable. The rotatable lid is vacuum sealed by means of a double Tec-ring (Tec Seal Corporation) arrangement similar to that described in (LEE 69). A Tec-ring is an O-ring made of graphite impregnated teflon. The teflon ring has a stainless steel helix at its core to give the ring springiness. The graphite lubricates the surface to facilitate rotation. The gap between the Tec-rings is differentially pumped by the same mechanical pump which pumps the slide valve stem seals. The vacuum system is vented through a small bellows seal valve located in one of the ports of the titanium well.

c. Detector Chambers

The pumping system for the detector chambers is located on top of the rotatable lid. Each of the two chambers is pumped by a Janis liquid helium cryopump, a 20 liter/sec Ultek Model 22-020 ion pump, and an Ultek Model 10-490 titanium sublimation pump. The ion pumps were added when

the detector isolation valve was installed, and since that time the titanium pumps are rarely used. They aid in the initial pump-down of the detector and are useful if small air leaks develop during the course of an experiment. They have much higher pumping speed for atmospheric gases than the ion pumps do, but when the cryopumps are charged, this additional speed is unnecessary. It is deceptive to state that the total speed of the pumps in each detector chamber is in excess of 5,000 liters/sec, because the speed at the electron bombardment ionizer (where it counts!) is severely limited by conductance to the pumps. Both detector chambers are necessarily small in the regions of the apertures and the ionizer. The distance across each chamber is a few inches and the chambers are crowded together to reduce $1/R^2$ intensity losses of the product beam. Consequently it is impossible to locate the pumps directly above their respective chambers. Molecules must negotiate several corners to get to the pumps. The passages to the pumps are constricted at the bends in our chambers and conductance is greatly reduced. If the main chamber had considerably more height, the additional volume could be effectively utilized to increase the conductances.

High speed pumping for condensibles in the region of the ionizer is provided by a liquid nitrogen filled copper box which surrounds the ionizer on three sides. This arrangement does not have all the advantages of the "fly-through" design described in (LEE 69), but nevertheless has a large favorable effect on the background level. Liquid nitrogen connections for the cold box are made inside the vacuum using nickel gasket Cajon couplings. Nitrogen is supplied by a gravity feed dewar located on the lid (Linde CR-10).

All detector pump gaskets are copper while indium wire gaskets seal the detector chamber to the lid and the back flange to the detector chamber. A gasket made of viton rubber sheet seals the detector aperture. Rubber O-rings are used in the bellows valves between the ion pumps and the titanium pumps. No noticeably high background signals result from this limited use of rubber.

E. Detector

A block diagram of the "universal" detector is shown in Figure 4. This chapter discusses the scheme depicted in the diagram. Neutral particles entering the detector are ionized by electron bombardment. The ions are extracted and focused by an einzel lens into an electrostatic spherical lens which bends the beam 90° into a quadrupole mass filter. Mass selected ions are accelerated and focused onto an electron multiplier where each ion initiates a detectable pulse of electrons. These pulses are amplified and counted by gated scalers which are synchronized with the modulation of one of the beams. The overall efficiency of the detector is estimated to be $\sim 5 \times 10^{-4}$. The greatest losses are due to the low efficiency of electron bombardment ionization which is at best a few tenths of a percent.

E - 1. Electron Bombardment Ionizer

The ionizer is shown in Figure 5. Brink's design (BRI 67) was adopted with slight modifications. The most desirable features of this design are the "long" ionizing region (filaments parallel to the beam

Figure 4

Block Diagram of "Universal" Detector

The detection scheme shown here is discussed in Section I-E of the text. Typical operating conditions are given next to each detector element. The voltages on the 5 cylindrical lenses shown just above the quadrupole mass filter all have units of kilovolts. The ionizer, extractor, and einzel lens are shown in detail in Figure 5.

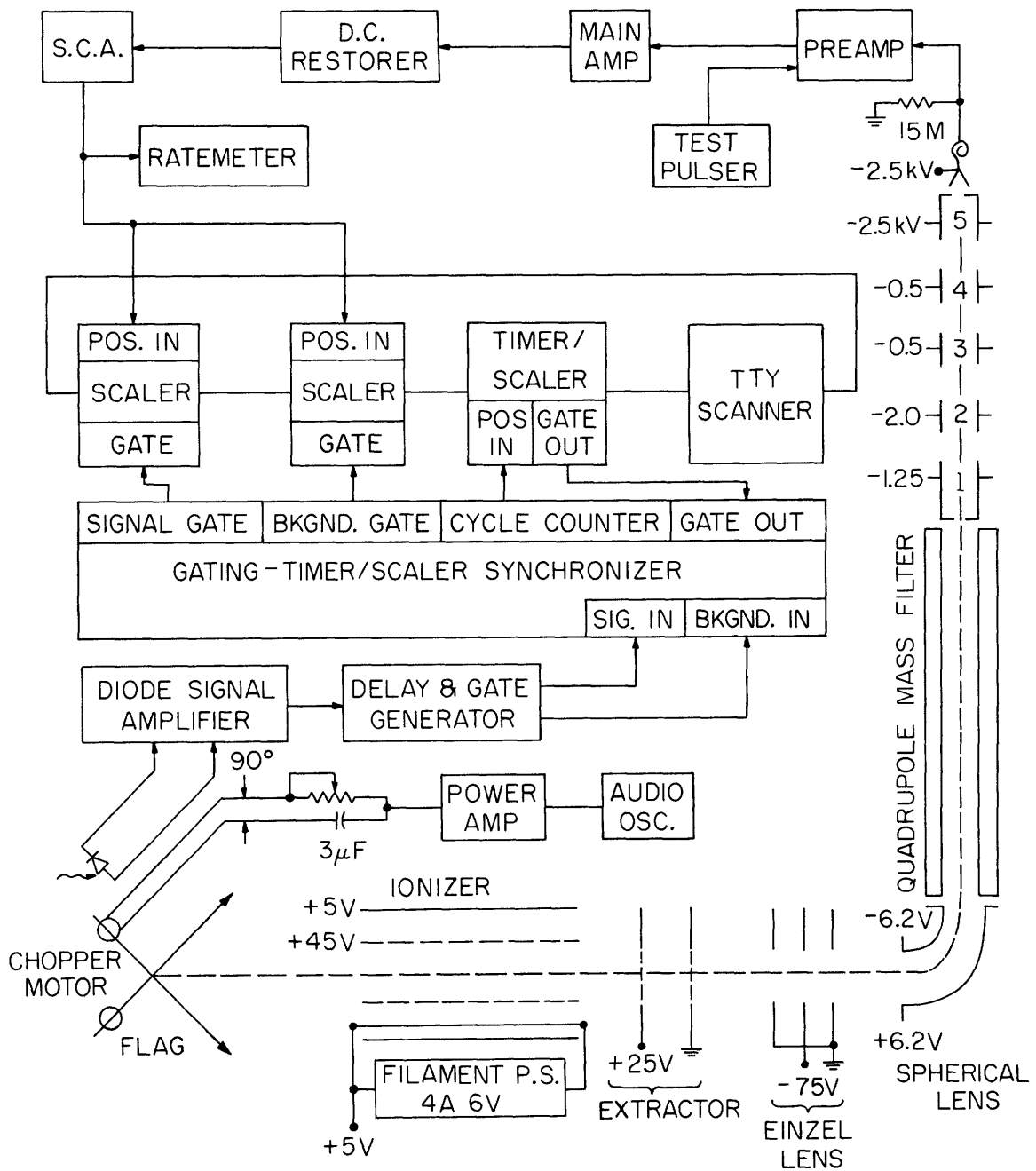
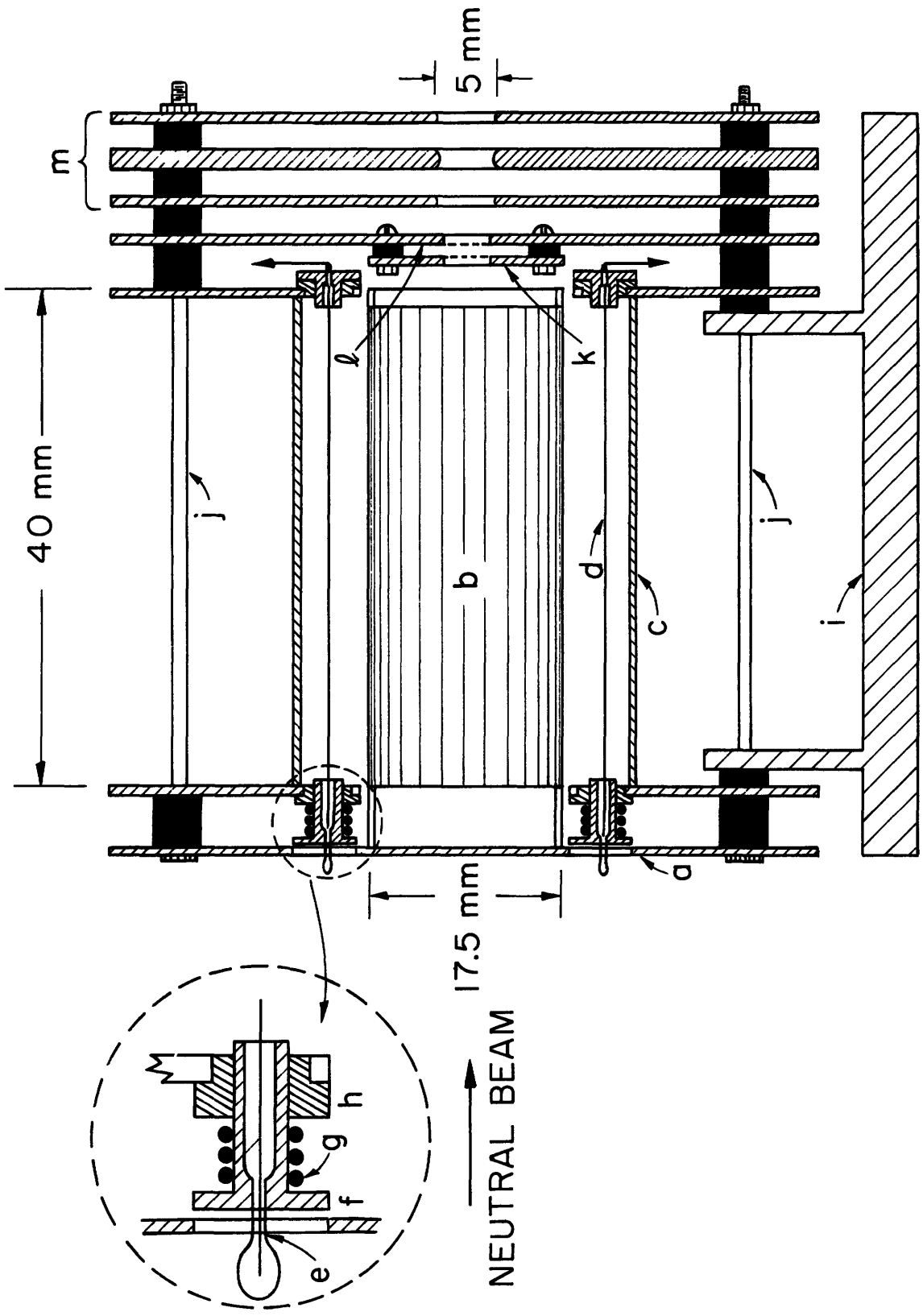


Figure 5

Electron Bombardment Ionizer

- a. Grid support plate. The 3.8 mm diameter ionizer entrance aperture is omitted.
- b. Cylindrical Grid
- c. Cylindrical Repeller
- d. One of four .008" dia. tungsten wire filaments.
- e. Metal tab is spot welded to the filament while the spring (g) is compressed.
- f. Stainless steel filament guide slides in boron nitride insulator (h). When filament is hot, the guide extends through the hole in plate a.
- g. Tantalum wire compression coil spring expands to take up slack in the hot filament.
- h. Boron Nitride insulator
- i. Ionizer assembly support bench.
- j. Alumina support rods, precision ground
- k. Extraction grid 1
- l. Extraction grid 2
- m. Einzel lens

The arrow attached to the right-hand end of each filament denotes a nickel wire lead which is spot welded to the filament.



axis) and the convenient cylindrical geometry. The neutral product beam enters the ionizing region through a circular aperture. This region is surrounded by a cylindrical grid which accelerates electrons into the ionizing region. The grid bias determines approximately the potential at which the ions are formed. Four tungsten wire filaments (0.008" dia.), parallel to the grid axis, are equally spaced around the grid. The difference between the grid bias and the filament bias determines the electron energy. Any combination of filaments may be used but typically only one is operated. Electrons are accelerated toward the grid and reflected by the outer cylinder (Repeller) which is biased slightly negative with respect to the filaments. Electrons thus "bounce" back and forth through the ionizing region until they are collected by the grid. This current is a measure of the filament emission and is monitored continuously. A weak extraction field draws positive ions out of the ionizing region. Once extracted the ions are accelerated to ground potential at grid #2. Placing the extraction grids close together makes the field lines parallel to the axis of the ionizer by minimizing fringing field effects. This tends to collimate ions which are directed off axis as they enter the extraction field.

There are two requirements of the ionizer which are independent of the rest of the detector. (i) A substantial fraction of the neutral particles entering the detector must be ionized and collected. (ii) The ionization efficiency must be independent of the neutral flux into the detector. In addition the ion beam must (iii) have an energy of less than 50 eV for adequate mass separation in the quadrupole and (iv) have an energy spread of only a few volts for high transmission through the spherical lens.

Most discussions encountered in the literature dealing with electron bombardment ionizers concentrate on the first requirement (i). They correctly emphasize the fact that large electron fluxes and electron dominated space-charge are desirable not only in maximizing the ionization efficiency but also in creating a potential minimum on the grid axis which aids in extracting positive ions. Unfortunately the second requirement (ii) precludes the utilization of large negative space-charge. Electron space-charge contributes to the potential field inside the grid and therefore affects the focusing for ion extraction. Space-charge neutralization varies directly with the neutral flux and therefore so does the extraction efficiency. Electron emission must be kept low enough so that this does not present a major problem. One way around this problem would be to use a very strong extraction field so that changes in space-charge would cause only small perturbations in the focusing. Unfortunately this results in large potential gradients in the ionizing region which widens the energy spread of the ions (iv) beyond acceptable limits. A compromise is reached between the desirability of high ionization efficiency and the need to suppress undesirable space-charge effects. Space-charge effects are most pronounced at high fluxes close to one of the beams. Normal operation of the ionizer allows measurements to be made to within $\pm 7.5^\circ$ of each beam. Measurements can be made closer but the electron emission must be drastically cut. Since the range mentioned depends on the pumping speed for the particular beam particles of interest, it should not be taken as an absolute value for every experiment.

The operating conditions of the ionizer are determined by a maxi-

mization of the signal to noise ratio for a particular reaction product. No simple model can explain the optimum settings for the various elements. A couple of examples will serve to illustrate this point. In the experiments which have been performed to date the optimum electron energy (grid bias minus filament bias) was found to be ~ 35 eV whereas reference to tables of ionization cross sections versus electron energy shows that the ionization cross section peaks between 100-150 eV. Also we found that operating at less than the maximum electron emission gave better signal to noise.

The ionizer is constructed of type 304 stainless steel sheet and tubing. The grid surrounding the ionizing region is made by spot welding platinum wires between two stainless steel rings which form the ends. The grid is then spot welded to the front plate of the ionizer. The repeller is a stainless steel cylinder which has approximately 50% of its surface area drilled out to increase the pumping speed in the ionization region. Tantalum wire compression coil springs maintain filament tension. By not passing current through the springs as is commonly done their useful lifetime is increased. Insulators are alumina, boron nitride, or steatite. All ionizer elements are stacked on alumina rods and spaced with alumina tubes ground to size. The entire assembly is screwed together and mounted on the detector bench as one unit. All electrical leads are bare copper wire, insulated where necessary with ceramic beads or tubing. The apertures of the extraction grids are covered with electroformed nickel mesh (150 lines/inch) which has been spot welded in place.

E - 2. Einzel Lens

As shown in Figure 5 the einzel lens is part of the ionizer assembly. The lens consists of three apertures equally spaced. The outer two plates are maintained at the beam potential (Ground) so that the ion energy is not altered by the lens. The inner electrode potential determines the focal length and can be adjusted to give maximum transmission through the spherical lens. In practice variation of the inner electrode voltage over a range of almost 50 volts on either side of the maximum has little effect on the signal transmitted through the entire detector. This behavior is expected. The principles of operation and a discussion of design parameters of the lens are discussed in (SPA 48) and (SEP 67). The reader is referred to these articles for further detail.

E - 3. Spherical Lens

The function of the spherical lens is to deflect the ion beam 90° with minimum losses. This enables the quadrupole mass filter, the final stage of accelerating lenses, and the electron multiplier to be mounted vertically. Although not necessary, this scheme saves a considerable amount of space in the main chamber and allows for easy electrical access to the detection components which project up through the rotatable lid. These advantages justify the use of the spherical lens since losses incurred in deflection are small compared to those due to the electron bombardment ionization efficiency.

In addition to deflecting the ion beam, the spherical lens has bi-directional focusing properties for a diverging beam, making it more

ideal than a cylindrical condenser lens which gives focusing only in the radial direction (PUR 38, MCD 63).

The trajectory of a charged particle through an electrostatic field depends on its kinetic energy. Every electrostatic lens exhibits focusing distortions due to the energy dispersion of the beam. In analogy to geometrical optics where light rays of different wavelengths have different focal lengths, this energy distortion is called chromatic aberration. Whereas the energy dispersion of spherical lenses has been successfully exploited for the purpose of energy analysis of ion beams, our application demands that the dispersion be reduced to a minimum. A first order theory predicts that the energy dispersion is proportional to the radius of curvature of the lens (PAO 67, MCD 63). Consequently the lens should be made as small as possible. One should keep in mind however that the simple theory breaks down as the radius of curvature approaches the spacing between the electrodes. Within this theory the energy resolution, $\Delta E/E$, is a constant. For the maximum ion energy acceptable to the mass filter, ~ 50 eV, the energy spread in the beam must be only a few volts for high transmission through the spherical lens. Even if a large portion of the ions are transmitted, the divergence of the beam will be increased by the dispersion, and this reduces the transmission through the mass filter. Given our present design these factors point out the importance of having a small energy spread in the ion beam. However the fact that $\Delta E/E$ is constant suggests that accelerating the ion beam to higher energy would relax the requirement on the energy spread. After passage of the beam through the spherical lens with high transmission and minimum divergence, a stage of deceler-

ating lenses could be used to inject the ions into the mass filter at the proper energy. There are other advantages to this scheme as well. If a larger energy spread were tolerable, higher extraction voltages in the ionizer could be used to increase the extraction efficiency and possibly reduce space-charge effects (see Section E - 1.). In addition the focusing of every lens would be improved at higher energy since chromatic aberration of the lens varies inversely with the voltage (SPA 48). Although presently the necessary decelerating lenses do not exist, serious consideration should be given to this scheme if major changes are made on the detector. Of course mounting the ionizer directly below the mass filter would eliminate the need for a 90° deflection lens altogether. Ions could be extracted vertically. However I believe that any major change in the detector should also include placing the ionizer in a separate chamber as described in (LEE 69) to gain the advantages of a "fly-through" design. This would be virtually impossible with the ionizer directly below the mass filter.

The lens consists of two 60° x 90° spherical segments, with radii of $0.9 \pm .0005$ " for the convex surface and $1.1 \pm .0005$ " for the concave surface. The electrodes are made of type 304 stainless steel and insulated from their mountings by $1/8$ " diameter sapphire balls. For the dimensions of our particular lens, the theoretical value of the focusing voltage, V_f , for a particle with kinetic energy, E , is given by: $V_f = 0.4E$ (PUR 38). The experimental value is very close to the predicted value (GEN 67). The voltage on the convex electrode is $-V_f/2$ and that on the concave electrode is $+V_f/2$. Beam particles at ground potential which enter the lens midway between the electrodes do not change energy as

they enter the field.

E - 4. Quadrupole Mass Filter

The quadrupole mass spectrometer is ideally suited to the requirements of the "universal" detector. It has numerous advantages over the magnetic mass analyzer, not the least of which is its compact size, enabling it to be easily incorporated into a rotatable detector. Other favorable factors are its relatively large entrance aperture and relative insensitivity to ion energy spread. Most importantly the resolution can be varied with a potentiometer to fit the requirements of the experiment. Since the resolution and transmission are inversely related, extremely high transmission can be achieved in cases where resolution is not an important factor.

The original literature references are PAU 53, PAU 55, and PAU 58, but the best discussion of the operating principles and the details of our particular commercial unit are found in the manual supplied by Extranuclear Laboratories. Points worth mentioning here are the factors which influence the ionizer and ion optics design.

Ions of the correct e/m (charge to mass ratio) spiral down the axis of the quadrupole and emerge from the exit aperture. Ions of incorrect e/m follow paths of exponentially increasing radii and are removed from the quadrupole axis. For mass separation to occur, the ions of incorrect e/m must remain in the transverse fields long enough to miss the exit aperture. The maximum allowed axial energy for unit mass resolution in a quadrupole 9" long operated at a typical frequency of ~ 1.5 MHz. is roughly 50 eV.

The maximum distance of an ion's trajectory from the axis depends on its initial distance from the axis and its transverse energy. The distance increases as the resolution is increased. Even ions of the correct e/m can be removed if they are injected too far off-axis with too much transverse velocity. Approximate equations for the upper limits of these factors are found in the operating manual and serve as guidelines in the design of ion optics.

The operation of the quadrupole mass filter has not been trouble-free, and since the problems either still exist or may recur at any time, they warrant mention. We have been perfectly satisfied with the electronics, but the mechanical design of the poles has caused two major problems. (i) The poles are not well insulated from the case. The original insulators were made of boron nitride and were only 0.020" thick. Possibly due to contamination by iodine, the surface of these spacers broke down continually at high voltage levels. New ones were made of aluminum oxide, efforts were made to clean up the vacuum, and these measures eliminated the problem, at least temporarily. Extra-Nuclear Laboratories informed us that more recent models have thicker insulation. (ii) A more intractable problem involves the power coupling to the poles. The exact cause of the trouble is not known, but the symptoms are large spurious ion signals coming from somewhere in the quadrupole when the power input is high. The signal is definitely an ion current and not RF pickup. The power connection to the poles is made through a stainless steel pointed rod pressed up against a steel strap which is screwed to the poles. A likely trouble spot is the junction of the pointed rod and the strap. A more permanent connection,

one less susceptible to arcing, might alleviate this problem.

E - 5. Final Focusing and Accelerating Lenses

Mass selected ions exiting the quadrupole have gained transverse kinetic energy. A final stage of lenses is necessary to refocus the ions and accelerate them to the energy required for efficient detection. A stack of five cylindrical tube lenses are located between the quadrupole and the electron multiplier. Typical operating voltages are shown in Fig. 5, and an excellent discussion of tubular lenses is found in (SPA 48).

E - 6. Ion Counting System

a. Channeltron Electron Multiplier

Various pulse counting techniques are available for detecting individually every ion reaching the detector. These techniques differ mainly in the way in which ions are converted to voltage signals. Schemes which have been successfully used in molecular beam experiments include the secondary electron-scintillator-photomultiplier chain (LEE 69), the secondary electron-semiconducting wafer combination (GEN 67, GOU 66), and the electron multiplier. The most important factors affecting the performance of pulse counting devices are efficiency and gain. The gain must be high enough to allow for discrimination against electronic noise without concomitant loss of signal pulses. The gain need not be particularly stable, however.

Originally the detector in our apparatus was a lithium drifted silicon, Si(Li), semiconducting wafer (GEN 67) preceded by an aluminum secondary electron surface. Repeated malfunctioning of the semiconducting wafer, purchased from Kevex-Ray Corporation, caused us to replace it with an electron multiplier. This was followed by several episodes where the Sorenson 30 KV D.C. power supply which biased the secondary electron surface literally burned up. Consequently, the aluminum surface was removed, and positive ions were collected directly by the multiplier. A Bendix Channeltron Electron Multiplier (capped output) was chosen because it had been successfully used in our laboratory to count K^+ ions from a surface ionization detector. It has advantages over other types of electron multipliers in that it can be exposed to atmospheric pressure and requires only one high voltage lead. It demonstrates high efficiency (EGI 69, BUR 67), has an initial gain greater than 10^7 , and an output pulse width of ~ 40 nsec. I contend that the only advantage the other two detection schemes mentioned above have over the Channeltron is negligible gain fatigue. We found that after about a year of operation the gain had fallen below the level necessary to discriminate electronic noise from signal pulses, and a new Channeltron was installed. However the cost is small compared to the operating expense of the apparatus, and the relative simplicity of the Channeltron argues strongly in favor of its use.

It should be mentioned in passing that Professor Yuan Lee pointed out to us after the Channeltron had been installed that the problems we had with the semiconducting wafer might be related to our failure to keep it reverse biased when not in operation. Apparently reverse biasing keeps

the lithium atoms in place and preserves the intrinsic properties of the doped semiconductor.

b. Pulse Counting Electronics

The detector electronics are shown in block diagram in Fig. 4. They consist of Canberra Industries' "1400 Series of Modular Nuclear Instruments". The most important consideration in choosing pulse counting electronics is the maximum counting rate possible. The output pulse width of the Channeltron is ~ 40 nsec and this sets an upper limit on its count-rate capability. Suppose for the sake of a rough estimate that there is a 50 nsec deadtime per pulse. That is to say that if two ions arrive at the multiplier within 50 nsec of each other they will be recorded as a single pulse. If 10^6 ions/sec are incident on the detector, then there will be 50 msec of deadtime per second of counting time. 5% of the signal will be lost on the average. In order to make full use of the range of the Channeltron, the electronics must be fast enough to handle at least 10^6 pulses/second. The Canberra electronics are not that fast but are suitable for almost any reactive scattering experiment. Typically reactive signals fall between one and a few hundred counts per second. The total count-rate arriving at the detector (signal plus background) must not exceed a few kilohertz to allow extraction of the signal in a reasonable length of time. High count-rate capabilities only become necessary when the true signal is ten or a hundred times larger such as might be the case in elastic scattering experiments.

The maximum count-rate of the Canberra system is limited by the relatively slow fall time of the preamplifier. The output of the preamp is a tail pulse with a rise time less than 50 nsec. and a 50 μ sec. fall

time. Since the main amplifier differentiates the preamp output, it does not "see" the slow fall time. However the DC level at the preamp output builds up if the pulses come too close together. Each successive pulse adds before the previous pulse returns to zero. This effect saturates the preamp at count-rates above ~ 50 kilohertz.

The main amplifier output is an adjustable gaussian pulse with a minimum deadtime of ~ 2 μ sec. Therefore using a faster preamp would not increase the count-rate capability of the system by very much.

The D.C. Restorer improves the count-rate performance by correcting for base line overshoot and re-establishing the system baseline to the initial level whenever a true pulse is not detected.

The Single Channel Analyzer (SCA) is a noise discriminator. The Channeltron pulse amplitude distribution is such that very few signal pulses are lost if the discrimination level is set at one-tenth the most probable pulse amplitude at the amplifier output. Typically the main amplifier gain is set to give a most probable pulse height of 1.5 volts. Under these conditions the electronic noise is usually 0.05 volts. Therefore discrimination at 0.15 volts satisfies the requirements of the Channeltron and rejects all electronic noise. For every input pulse above the discriminating level, the SCA puts out an 8 volt pulse, 0.4-2.5 μ sec. wide. These pulses are fed into two gated scalers and a linear ratemeter.

The Timer/Scaler is the master of the data collection. Its START button initiates the counting by enabling the scalers for a preset number of chopper cycles (count mode) or a preset time (time mode).

After each counting period is terminated by the Timer/Scaler, the Teletype Scanner transmits the serial BCD (Binary Coded Decimal) outputs

of the scalers, the Timer/Scaler, and two digital voltmeters either to a model 33 Teletype or a PDP-8/L computer.

F. Beam Modulation System

Beam modulation and phase sensitive detection have become standard techniques in molecular beam scattering experiments. Several references to various applications can be found in (BIC 70). The justification for such techniques was given in Section I - B above and is not repeated here. A block diagram of the beam chopper is shown in Fig. 4.

F - 1. Rotary Chopper

A slotted cylinder rotated about its symmetry axis chops the beam at twice the driving frequency of a hysteresis synchronous motor (Globe 53A118-2). The beam is modulated typically at 100 Hz. A Dynakit Mark III 40 Watt audio amplifier amplifies the sine wave output of a Krohn-Hite 440 AR oscillator and drives the Globe motor. The 90° phase shift required by the motor is supplied by a capacitor. The potentiometer in the amplifier output equalizes the amplitudes in the two leads. The power to the motor is controlled by the variable output of the oscillator and is always operated at the minimum power necessary to keep the chopper in sync.

The chopper is located in source differential pumping chamber 2.

F - 2. Diode Signal Amplifier

A light and photodiode arrangement provide a reference signal for the scaler gates. A schematic of the diode signal amplifier is shown in Fig. 6.

Figure 6

Schematic Diagram of: Photodiode Signal
Amplifier, Delay and Gate Generator, and
Synchronizer

Each section of this circuit is described separately in the text.

Diode Signal Amplifier

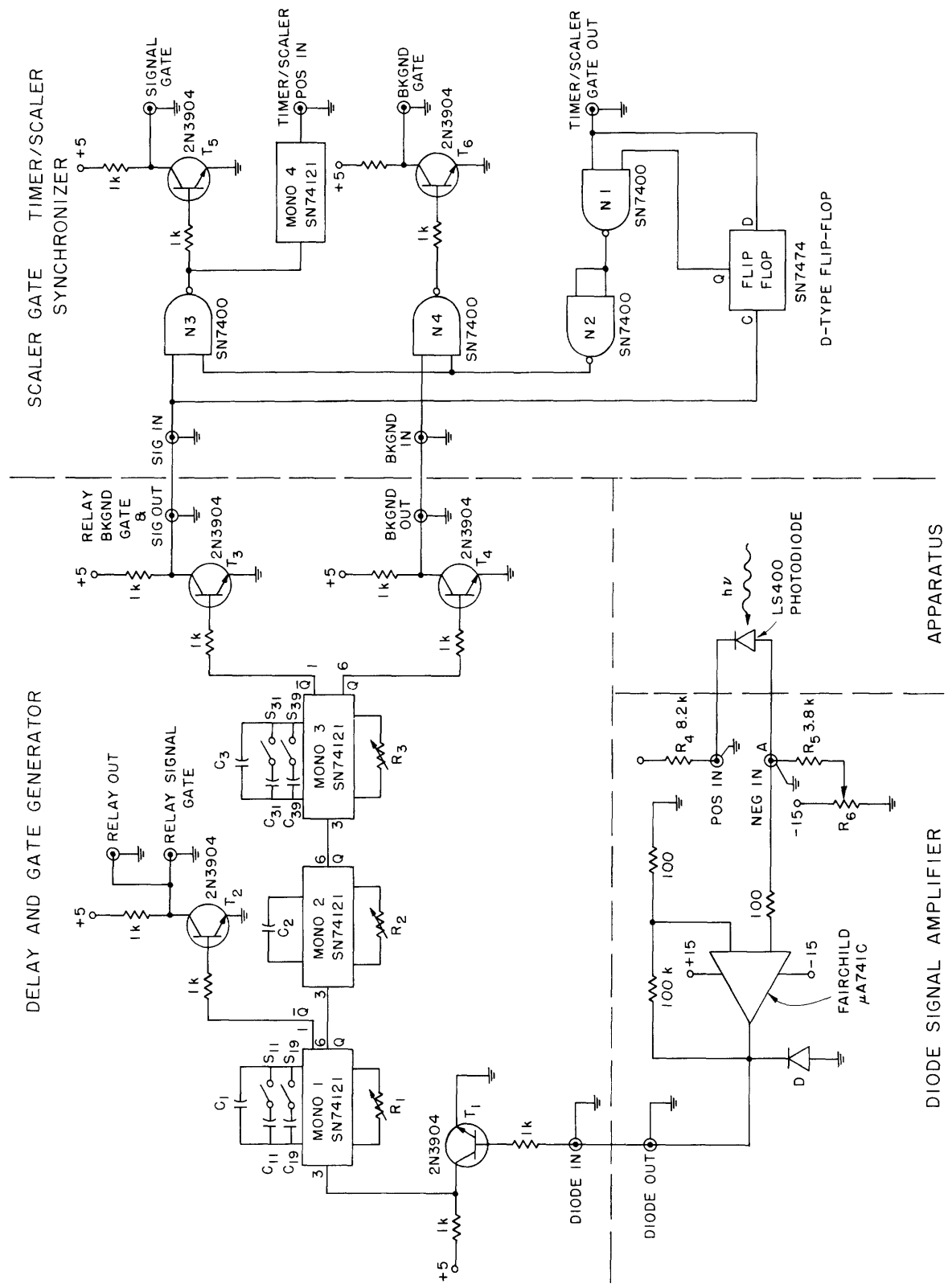
The terminal just above R_4 should be labeled V_{DS} (+ 15 volts).

Synchronizer

N3 output is connected to pin 3 of mono 4.

Q output (pin 6) of mono 4 is used.

Each circuit bounded by the dotted line occupies a separate chassis in the electronics racks.



SCALER GATE TIMER/SCALER SYNCHRONIZER

DELAY AND GATE GENERATOR

APPARATUS

DIODE SIGNAL AMPLIFIER

The circuit is a voltage divider with two operating states followed by a non-inverting amplifier with a gain of 1,000. Such high gain is not necessary but it insures that the amplifier saturates quickly when the diode begins to conduct. When the diode is non-conducting, R_6 is adjusted to set point A to ground potential. R_6 corrects for small leakage currents in the diode which might raise the voltage at A high enough to saturate the amplifier. When light causes the diode to conduct, the voltage at A is determined by R_4 , R_5 , and V_{DS} . The diode D clips the negative portion of the amplifier output. The output waveform is a positive going square wave which fires once for every chopper cycle.

F - 3. Delay and Gate Generator

A schematic of this circuit is shown in Fig. 6, and the timing sequence of the circuit is depicted in Fig. 7. The reference diode signal is delayed by MONO 1 (monostable multivibrator) to account for any constant phase, ϕ , between the modulated beam and the diode signal and for the flight time of the beam from the chopper to the detector. The delay time can be varied by toggling in C_{11} and C_{19} and adjusting R_1 . The output of MONO 1 is a square wave whose falling edge is in phase with the modulated signal reaching the detector.

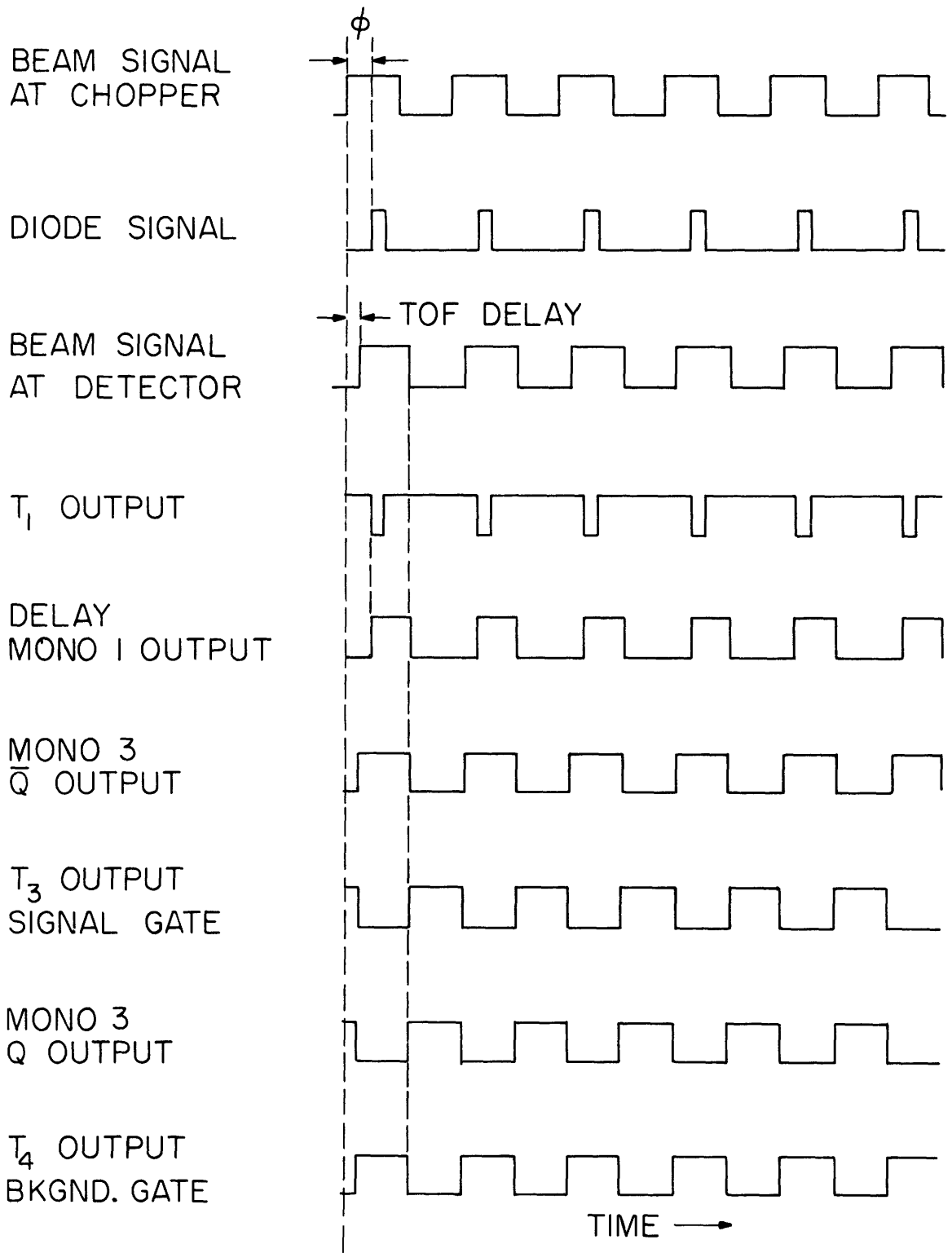
MONO 2 is added to the circuit for another application which is mentioned below. In this circuit its effect is nil. C_2 is disconnected and R_2 is set to zero. MONO 2 triggers off the falling edge of MONO 1 and puts out a 40 nsec square wave.

MONO 3 generates the signals which gate the scalers on and off. The

Figure 7

Timing Diagram of Delay and Gate Generator

Voltage vs. Time is plotted for several points in the circuit shown in Figure 6. There is a mistake in this figure. The Beam Signal At Detector should be inverted so that the falling edge of Mono 1 Output coincides with the rising edge of the Beam Signal At Detector. This gives the proper zero phase between the Beam Signal At Detector and the Signal Gate. The discussion in the text (I-F. 3) is not affected, because the photodiode signal is used as a reference point for the discussion and not the signal itself.



external capacitance and resistance are adjusted to give a square wave output with 50% duty cycle. Since the width is variable this circuit can be adapted to a wide range of chopping frequencies. The \bar{Q} output, after inversion by T_3 , is a square wave in phase with the signal reaching the detector and it gates the signal channel scaler. The Q output is the inverse of \bar{Q} and when inverted by T_4 is exactly 180° out of phase with the beam signal. This of course is the background channel gate.

F - 4. Scaler Gate - Timer/Scaler Synchronizer

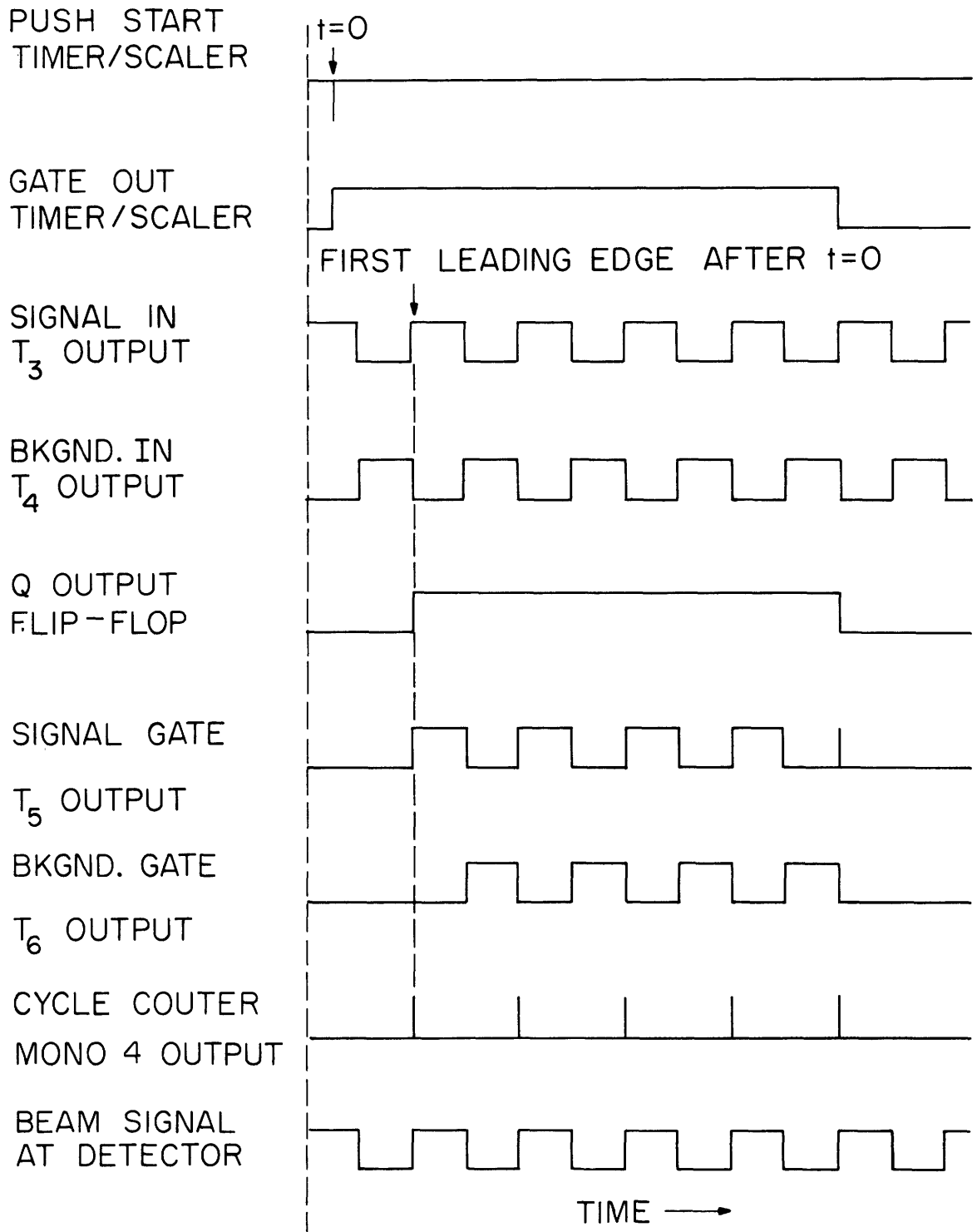
The synchronizer eliminates any error, however small, due to pushing the START button on the Timer/Scaler during the middle of a chopper cycle. Ordinarily the scaler whose gate is high when the START button is pushed immediately begins to accumulate counts. In this way one channel could be open for as much as one-half chopper cycle longer than the other channel in any given counting time. Although this error is insignificant in most cases, this circuit insures that both channels are open for exactly the same time.

The timing sequence and the circuit are shown in Figs. 8 and 6 respectively. Logic truth tables for the integrated circuit components are found in the "TTL Integrated Circuits Catalogue from Texas Instruments (#CC201)". Points to note in Fig. 8 are: (i) Both gates are low (scalers inhibited) before the START button is pushed. (ii) The first leading edge of the Signal In waveform, after the START button is pushed, triggers the flip-flop which allows the input signals to pass the nand gates (3 and 4). Thus the scalers begin accumulating counts exactly in phase with the signal.

Figure 8

Timing Diagram of the Scaler Gate-Timer/Scaler
Synchronizer

Voltage vs. Time is plotted for several points in the synchronizer circuit shown in Figure 6. Discussion of the synchronizer is in the text (I-F. 4).



(iii) When the Timer/Scaler has registered n preset counts, the scalers have accumulated pulses for exactly $(n-1)$ complete chopper cycles. (iv) When the preset number of counts is registered on the Timer/Scaler, the GATE OUT signal goes low, the flip-flop changes state, and nand gates 3 and 4 block the gating signals.

F - 5. Relay Beam Flag and Chopper

The beam which is not modulated may be interrupted in the second differential pumping chamber by means of a flag attached to the movable tongue of a relay. When the solenoid is energized, the flag is pulled out of the beam path. This device may also be used to modulate the beam at very low frequencies (1-4 Hz). The flag and circuit for driving the relay are shown in Fig. 9a. The upper left-hand corner of the figure shows the switching circuit for manual flagging. When the switch is closed, the capacitor discharges through the relay giving a current transient which energizes the solenoid. The voltage across the relay falls to a low D.C. level which is just enough to hold the flag out of the beam path. When the switch is opened, the flag springs back to interrupt the beam. The chopper circuit is essentially the same with the toggle switch replaced by two transistors. Fig. 9b shows the energizing waveform for the relay as well as the timing sequence for the gates.

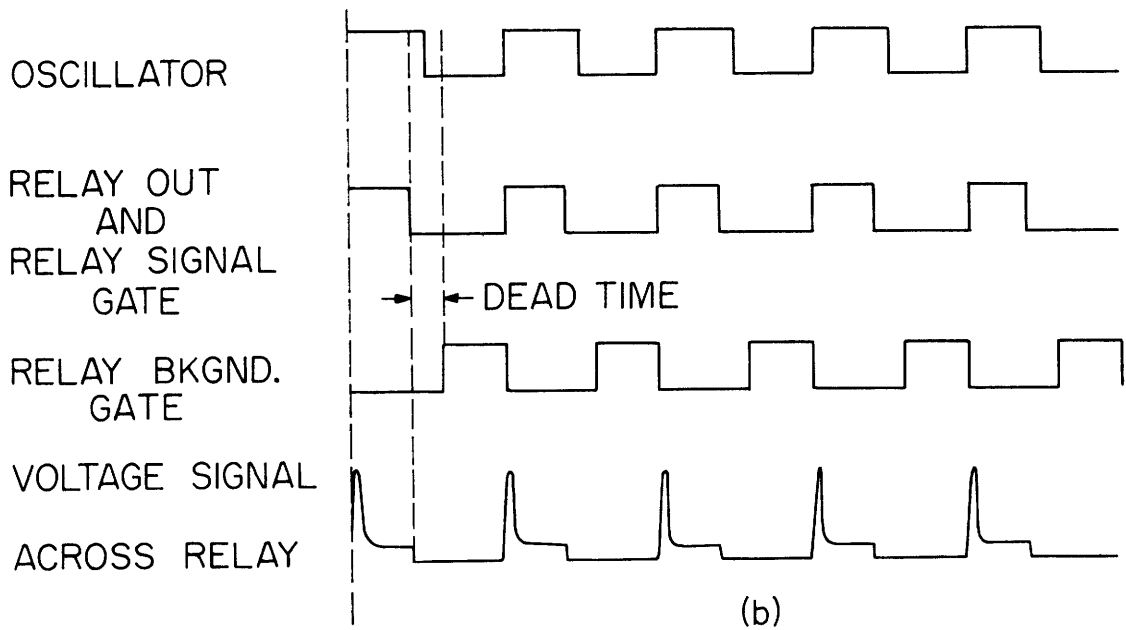
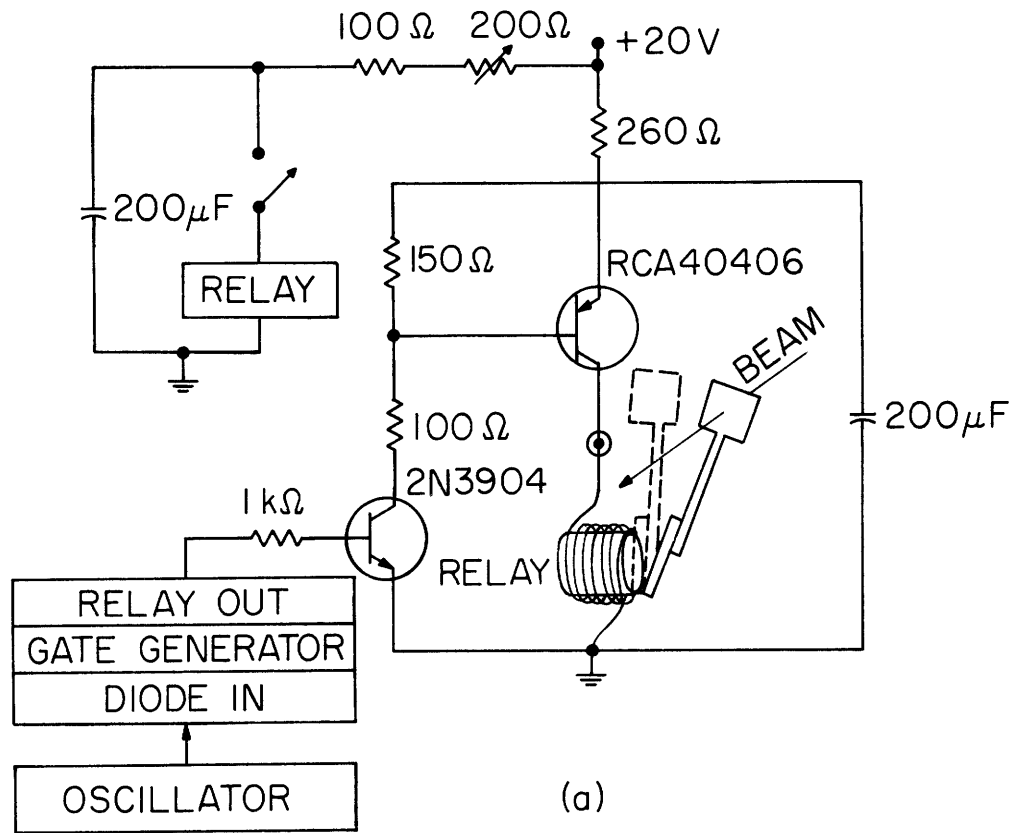
Ordinarily the relay flag is not used to modulate the beam, but the gating circuitry has been constructed. For low chopping frequencies each half cycle (Beam ON and Beam OFF) is long compared to the flight times of molecules, and no time of flight (TOF) delay is necessary. The square wave output of a Krohn-Hite 440 AR oscillator supplies the desired frequency.

Figure 9

- a) Relay Beam Flag and Chopper Circuit
- b) Timing Diagram for Relay Chopper

- a) The junction just below the 260 ohm resistor is connected and this should be denoted with a heavy dot at the junction.
- b) Voltage vs. Time is plotted for several points in the gate generator circuit in Figure 6.

Discussion of the chopper circuit is in the text (I-F. 5).



This signal is connected to the Diode In input of the Delay and Gate Generator (Fig. 6). The duty cycle of the modulation is determined by MONO 1. The \bar{Q} output, once inverted, is the relay driving signal and the signal channel gate. MONO 2 may be adjusted to give a deadtime between the gates when the modulation duty cycle is less than 50%. The \bar{Q} output of MONO 3 is the background gate. The gates are synchronized with the Timer/Scaler just as they are when the rotary chopper is used.

Part II

MOLECULAR BEAM STUDY OF POLYATOMIC
FREE RADICAL REACTIONS

A. Introduction

After almost two decades of experimentation molecular beam research is only just beginning to fulfill the promise made to the chemical community that beam "kinetics" would contribute significantly to many areas of "traditional" chemistry, providing new insights on a microscopic level into old problems. Several laboratories are involved in this endeavor. The Harvard group under Herschbach is studying the nature of halogen atom displacement reactions in organic compounds such as allyl bromide. Studies at Chicago under Lee on fluorine atom-olefin reactions are beginning to answer questions about intramolecular energy transfer which relate directly to theories of unimolecular decomposition. In the same spirit of applying molecular beam techniques to an ever widening range of chemical problems, we have undertaken to demonstrate the possibility of studying polyatomic free radical reactions in crossed beams. The first successful results have recently been communicated (MCF 72).

The study of free radicals comprises a considerable portion of "traditional" chemistry. By the late 1800's, vapor density measurements had demonstrated the existence of atomic free radicals at high temperature. Nevertheless, the hypothesis that free radicals occurred as intermediates in many gas phase reactions at ordinary temperatures remained largely conjectural until the 1920's, when the now classic experiments of Wood (W00 20, W00 21, W00 22, W00 22b) on atomic hydrogen and Paneth (PAN 29) on methyl proved the transient existence of free radicals under relatively mild conditions. In spite of their importance, free radicals remain notoriously unyielding to direct study by conventional methods due

to their extreme reactivity. This characteristic makes them ideally suited for molecular beam experiments; and indeed, atomic free radicals have received a great deal of attention in molecular beam studies (see section I-A).

We pursued the logical next step, the study of simple polyatomic radicals, CH_3 and C_2H_5 . Presented here are measurements of the angular distribution of reaction products for $\text{CH}_3 + \text{Cl}_2$, Br_2 , I_2 , ICl and $\text{C}_2\text{H}_5 + \text{Br}_2$ reactions at thermal energy. These systems were chosen because of the relative ease of producing CH_3 and C_2H_5 in the gas phase and because of the expected relatively large cross sections ($\sim 1 \text{ \AA}^2$). Although these first measurements represent only a modest excursion into the vast territory of free radical chemistry, it is hoped that they serve as a bellwether to molecular beamists and as an omen of things to come to those impatient critics of molecular beam "kinetics".

B. Halogen Molecule Beam Source

The halogen beam originates from a typical nozzle source. The advantages, of course, of this type of source are high center line beam intensities accompanied by narrow velocity distributions. We were primarily concerned in the experiments reported here with obtaining beam intensities sufficiently high to observe reactive scattering. In each experiment the source pressure and nozzle-to-skimmer distance were optimized to give maximum signal at an electron bombardment beam monitor located in the main chamber ~ 18 inches from the halogen nozzle. This is the extent to which the beam was characterized. Information concerning the absolute beam

intensities and the velocity distributions is at best indirect. A beam attenuation measurement of a few percent was one indication of high intensity. An absolute flux can be estimated from the source pressure, size and geometrical arrangement of the nozzle and collimating apertures, and the beam monitor readings. These approximate calculations always indicated that the intensities were comparable to those obtainable by other workers. See for example Fig. 2 in (GOR 71). In this reference absolute intensity measurements are made on a potassium nozzle beam which show that up to about 50 torr pressure behind a .006" nozzle the center line intensity can be calculated from the effusive flow formula, and at increased source pressure the intensity levels off. We observe this leveling off and attribute it to background scattering in the source chamber. For bromine, this intensity saturation is observed above 100 torr source pressure (nozzle diameter .010"). Table I gives typical operating conditions for the halogen sources and their measured relative intensities. To convert beam monitor signals to relative fluxes, each current measurement must be divided by the halogen velocity (Table III) and by the electron bombardment ionization cross section. The ionization cross section is assumed to vary directly with molecular polarizability (LAM 57). The halogen polarizabilities are (in \AA^3): 4.6 for Cl_2 (HIR 54c), 6.2 for Br_2 (BIR 69), 9.7 for I_2 (BIR 67), and 7.5 for ICl (BIR 69).

The velocity distributions were not measured. Nevertheless, it is believed that an accurate value for the most probable velocity can be calculated and an upper bound for the width of the distribution easily estimated. In Fig. 2 of (McD 72) a measured iodine nozzle beam velocity distribution is given. The experimental conditions reported there are quite

Table I

Halogen Molecule Nozzle Beam Source
Operating Conditions

Halogen	Reservoir Temp, T_R	Vapor Pressure at T_R	Nozzle Temp. T_0	Source Chamber #1 Pressure (d)	Beam Monitor Signal
	$^{\circ}\text{C}$	torr	$^{\circ}\text{C}$	torr $\times 10^5$	Amps $\times 10^8$
Br_2	19	> 150 (a)	75	.8	2.8
Cl_2	room	Pressurized Gas	75	(e)	2
I_2	130	> 100 (a)	160	1	3
ICl	50	> 100 (b)	78	1	2

(a) (HON 60)

(b) (COR 42)

(c) Chromel-Allumel Thermocouple Readings

(d) Uncorrected Ion Gauge Readings

(e) Ion Gauge would not operate above $\sim 5 \times 10^{-6}$ in Cl_2 atmosphere

similar to ours. Within a few percent the peak velocity can be calculated by assuming complete conversion of transverse translational energy and rotational energy into axial motion. Assuming infinite Mach number M , the most probable velocity for this type of flow is given by $v_s = \sqrt{\frac{2kT_0}{m}} \sqrt{\frac{\gamma}{\gamma-1}}$, where k = Boltzmann's constant, T_0 = nozzle temperature, m = molecular mass, and γ = ratio of heat capacities ($7/5$ for diatomic gases). The first factor is the most probable velocity of a Maxwellian distribution in an oven at temperature T_0 . Even if the distribution is characterized by a Mach number as low as 6, the peak velocity is lowered only by $\sim 7\%$ from the value predicted with Mach infinity. For the purpose of constructing Newton diagrams, we assumed Mach 6 and calculated peak velocities using the formula:

$$v_s^2 = \frac{2kT_0}{m} \left(1 + \frac{\gamma-1}{2} M^2\right)^{-1} \frac{\gamma M^2}{2}$$

which reduces to the above formula if $M = \infty$ (OWE 48, ASH 66). The halogen beam velocities calculated in this way are given in Table III.

Based on a comparison of our operating conditions with those given for I_2 in (MCD 72), we estimate that the full width at half maximum is less than 15% of the peak velocity for any of our halogen beams.

The source tube and nozzle are constructed of type 304 stainless steel. Nozzles of various diameters were made and are easily interchangeable. The nozzle is held in place by a retaining nut; a soft metal gasket prevents even small leaks. The source is designed to be movable from outside the vacuum so that the optimum nozzle-to-skimmer distance can be found during an experiment. The front end or nozzle end of the source tube slides on pins as depicted in Fig. 2. The source tube extends through the vacuum wall

at the back of the source chamber and is vacuum sealed by a 0.5" O-ring compression seal. This O-ring is well greased and the source tube slides back and forth manually. A flexible monel hose connects the source tube to the gas handling system.

The skimmer for the nozzle source is made by rolling 0.001" tantalum foil into a 60° cone and grinding off the tip to form an orifice of ~ 0.040". The skimmer is heated with a Watlow cartridge heater to prevent condensation.

Typically, halogen vapor is passed from a reservoir located outside the vacuum wall of the apparatus through a Hoke metering valve, down the 20" long source tube, and out the nozzle. To prevent condensation the source tube and nozzle are heated ~ 25-50°C hotter than the reservoir. The heater is a .015" diameter tantalum wire insulated with fiberglass sleeving and wound around the source tube over its entire length. A variac supplies the power. For the I₂ and ICl sources additional heaters are necessary for the gas transfer tubing outside the vacuum since the reservoirs are heated above room temperature. Here conventional heating tapes suffice. All vacuum couplings in the gas handling lines are made with stainless steel Swageloks (teflon front ferules, stainless steel back ferules). These fittings never leaked during an experiment even when heated to 150-175°C for the I₂ source. After cooling down, however, they had to be retightened before the next experiment.

The only real difference between the individual halogen beam sources is the reservoir. For Cl₂ a Matheson cylinder is connected directly to the metering valve with a section of polyethylene tubing. The tank is regulated at ~ 5 lbs. pressure. Bromine (Reagent Grade), a liquid with a vapor pressure > 150 torr at room temperature, is the simplest to handle. It is easily

poured into a glass ampule in the fume hood with the aid of a glass funnel. The ampule is fitted with a teflon stopcock which connects to the metering valve. During an experiment the ampule is submerged in water which is gently heated (Watlow cartridge) to counteract evaporative cooling of the bromine. This simple scheme maintains the temperature slightly below room temperature to within 0.5°C . For I_2 and ICl , both solids at room temperature, the glass ampule is filled once again in the fume hood and connected directly to the metering valve. The low vapor pressure at room temperature compared to bromine obviates the need of a stopcock for transporting the material. The ampule is heated with a Watlow strip heater powered by a variac. Monitored with a thermocouple, the temperature reaches a steady value after ~ 1.5 hours of heating. The temperature of the reservoir is chosen so that the vapor pressure is higher there than in the source tube. This allows the flow to be metered down, providing a way to make small changes in the beam intensity without altering the source temperature.

The halogen beam intensity is monitored continually throughout an experiment. Corrections are made if the beam monitor collector current ever varies by more than a few percent. The stability of the halogen source limits the length of time of every experiment. Actual beam running time has a maximum of 8 - 10 hours. For bromine this corresponds to ~ 30 cc consumption. Although a careful study was never made, it is believed that the drastic intensity fall-off is due to the accumulation of halogens on surfaces cooled either directly by liquid nitrogen or indirectly through radiation to a liquid nitrogen cooled surface. Eventually the beam becomes completely blocked. Liquid nitrogen cryopumping accounts for almost 100% of the pumping speed in the halogen source chamber. After an experiment

there is a tremendous amount of halogen trapped in the source chamber and differential pumping chamber. To avoid disastrous contamination of the mechanical pumps, the slide valves isolating the diffusion pumps from the source chambers are closed at the end of each experiment. When the cold shields warm up, the halogens are trapped in cold fingers attached to the chambers. The traps are removed and allowed to warm up in the fume hood.

C. Alkyl Radical Beam Source

A rather large body of data on the mass spectrometry of free radicals has been reviewed by Lossing (MCD 63b). Several references cited in that review discuss simple methods for generating alkyl free radicals in the gas phase. The problem which we faced was generating them in sufficiently high concentrations in a beam to do reactive scattering experiments. The adoption of a pyrolysis source to generate highly reactive atomic free radicals from homonuclear diatomics was successful (see Section I-A) because at sufficiently high temperature dissociation equilibrium favors a large concentration of atoms. There is no temperature, however, where methyl radicals (or ethyl) are stable in an equilibrium source, regardless of the parent compound. To overcome this problem adequately, the source design attempts to minimize the residence time of the radicals in the high pressure dissociation region. This is accomplished by a fast flow of vapor through a short pyrolysis tube, followed immediately by expansion into the high vacuum where beam molecules suffer no collisions (KAL 69).

Many organometallic compounds of the general formula $(R)_n M$ where R is an alkyl radical, n an integer from 2 to 4, and M is usually a heavy metal

atom, have very low bond energies (40-50 kcal/mole) and undergo smooth unimolecular decomposition at fairly low temperature to produce alkyl radicals. Both $(\text{CH}_3)_2\text{Zn}$ and $(\text{CH}_3)_2\text{Cd}$ were used to produce CH_3 radicals and $(\text{C}_2\text{H}_5)_2\text{Zn}$ to produce C_2H_5 radicals in our studies. Considerations which led to these choices were commercial availability, toxicity, and the vapor pressure of the metal. We found in using $(\text{CH}_3)_3\text{Bi}$ that since the vapor pressure of Bi is lower than the source pressure at the operating temperature, clogging due to condensation was a serious problem. On the other hand, though Hg would not condense in the source, $(\text{CH}_3)_2\text{Hg}$ was rejected because of its well-known toxicity. Unlike $(\text{CH}_3)_2\text{Hg}$, $(\text{CH}_3)_2\text{Zn}$ and $(\text{CH}_3)_2\text{Cd}$ decompose rapidly in air, and we believe that the oxidation products are less hazardous than the parent compound.

Precautions are taken to minimize our exposure to these chemicals. $(\text{CH}_3)_2\text{Zn}$, $(\text{CH}_3)_2\text{Cd}$, and $(\text{C}_2\text{H}_5)_2\text{Zn}$, purchased from Alfa Inorganics, are shipped in stainless steel ampules which are sealed by needle valves. The ampule is attached directly to the gas handling system without being opened first. The compounds are never allowed to flow into the apparatus unless the pyrolysis tube is hot enough to give essentially complete dissociation. This rule is violated only when absolutely necessary for the purposes of an experiment.

The pyrolysis tube is mounted on the end of a source tube which is identical in construction to the halogen source tube discussed earlier. The vapor pressure of the organometallic liquids are conveniently high so that constant temperature of the reservoir can be maintained by means of an ice bath. The flow rate into the source tube is controlled with a Granville-Phillips variable leak valve. The pressure in the source tube is monitored

continuously with a Quartz Spiral Gauge (Texas Instruments).

A simple pyrolysis tube is mounted on the end of the source tube. The design evolved to a model adequate for the study of these halogen reactions (angular distribution measurements), but it cannot be said that the optimum design has been achieved. The pyrolysis tube is shown in Fig. 10. It consists of a cylinder ~ 1 " long, 0.2" diameter made by rolling up a piece of .001" thick Tantalum foil and spot welding the seam. The source is heated to $\sim 1,500^\circ\text{K}$ (bright orange) by passing current directly through the source wall. The entire source tube is heated enough in this way to prevent radiative cooling by the liquid nitrogen cooled surfaces which completely surround the source tube. The "crinkly-foil" in the end of the pyrolysis tube increases the thermal contact with the vapor. Without the "crinkly-foil" insert only a very small fraction of the gas is dissociated. Therefore one has control over the length of the effective pyrolysis region, and ideally it should be as short as possible consistent with the requirement of high dissociation efficiency. The pyrolysis tube and "crinkly-foil" are easily constructed and are replaced whenever appreciable clogging is observed after an experiment.

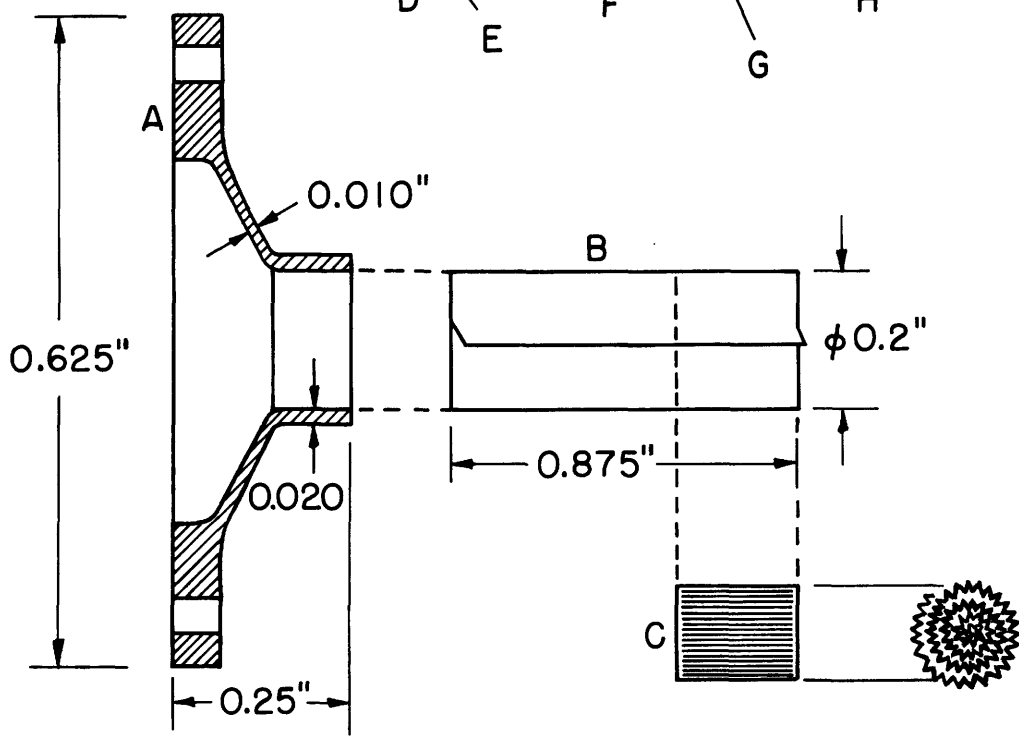
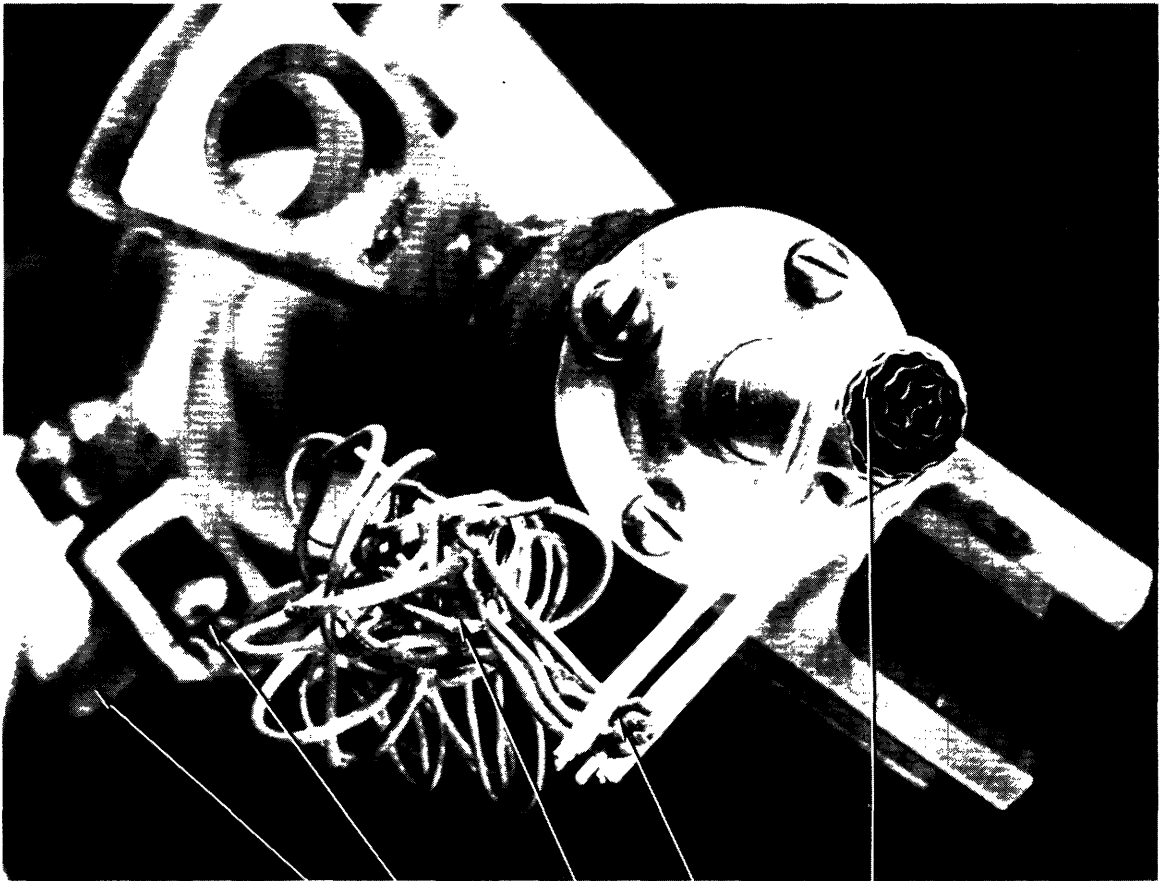
The operation of the source was tested and analyzed mass spectrometrically. Repeated scans (Quadrupole "Sweep" Mode) of the low and high mass spectrum of the beam were taken as a function of the heater current and source tube pressure. During these tests we observed the percentage decrease of parent organometallic peaks and relative increase of radicals based on a crude carbon balance. Analysis of the mass spectra indicates that the total beam flux is at best 7 - 20% radicals. Even though the radical concentration is very difficult to measure, the mass spectra for a given set of operating conditions were reproducible, indicating that the composition

Figure 10

Pyrolysis Source for Alkyl Radicals

- A. Type 304 stainless steel flange and holder for tantalum tube B.
- B. Tantalum tube is rolled up out of 0.001" foil, and slipped into holder, leaving about 5/8" of tube exposed.
- C. Crinkly-foil insert; made from piece of crinkly-foil, 1/4" x 15/8".
- D. Current lead, copper tubing (1/8" O.D., 0.03" wall).
- E. Mechanical connection between lead, D, and nickel wire leads, F.
- F. Flexible nickel wire leads take up any expansion strain.
- G. Spot welded connection between nickel wire leads, F, and 0.02" dia. tantalum leads.
- H. Four tantalum leads are spot welded to the end of tube B. Tantalum leads are used for final connection to tube B to insure that the end of the tube is not cooled by conduction through the leads.

The guides for the alignment pins can be seen in the upper left- and lower right-hand corners of the figure.



of the beam is constant with time as expected. The most direct method of optimizing the source conditions for radicals is to measure the reactive scattering signal as a function of the source parameters. Typical operating conditions determined in this way are 0.7-1.0 torr source tube pressure and 33 amps heater current (Ultek Boostivac Power Unit Model 60-504).

Major impurities in the beam consist of CH_4 , C_2 hydrocarbons, and atomic metal. Since small hydrocarbons are not pumped efficiently by liquid nitrogen cooled surfaces, the methyl source chamber pressure is always higher than the halogen source chamber pressure even though the actual gas load in the methyl chamber is less. The methyl source chamber ion gauge usually reads $\sim 7-8 \times 10^{-5}$ torr during an experiment.

The velocity distribution in the beam is assumed to be Maxwellian at a temperature of 1,500°K. The most probable velocity of such a distribution is used for construction of Newton diagrams. This corresponds to 1580 m/sec. for CH_3 and 1135 m/sec. for C_2H_5 .

D. Experimental Procedures

Each system studied is a variation on the same experiment: measurement of the laboratory angular distribution of reactively scattered alkyl halide products from alkyl radical and halogen molecule collisions. Therefore the conditions and procedures for each experiment are essentially identical.

The critical apparatus dimensions are:

Distance from the scattering center . . .

. . . to the alkyl radical oven	2.5 inches
to the first alkyl collimating aperture	2.0
to the halogen nozzle	2.6
to the halogen skimmer	2.3
to the second collimating sperture for both beams .	0.6
to the beam monitor entrance	15.6
to the first detector aperture	1.9
to the ionizer entrance	6.2

Beam defining apertures are interchangeable and in these experiments relatively large apertures were used:

Halogen skimmer	60° cone, 0.04" aperture
Halogen collimating aperture	0.15" dia., 0.25" long
First alkyl radical collimating aperture	0.20" dia., 0.04" long
Second radical collimating aperture . .	0.18" dia., 0.25" long
Detector apertures (2)	0.15" dia., 0.4" long
Beam Monitor entrance aperture	0.5"

One day prior to an experiment, the apparatus is evacuated. Both the main chamber "roughing" valve and the source chamber slide valves (all 4 of them) are opened initially. This enables the two largest mechanical pumps (Welch 1397) to evacuate the system. This "roughing" procedure can last up to two hours before the ultimate mechanical pump vacuum is reached. If this proceeds with no indications of a leak, the butterfly valve is opened and the 2" diffusion pump begins pumping on the system. The slide valves and the "roughing" valve in the main chamber are closed, and the 2" diffusion pump is allowed to work overnight. In the morning the main chamber pressure is

usually low on the 10^{-4} torr range if everything is alright. The four diffusion pumps are turned on first thing; the slide valves are opened when the diffusion pump side arms (foreline connections) become hot to the touch. When these valves are opened the main chamber pressure drops quickly an order of magnitude.

If all the liquid nitrogen transfer lines have not already been blown dry with compressed air this is done next. Several experiments ended abruptly when ice clogged a $1/4$ " transfer tube and could not be unplugged. 20-30 minutes of "blowing" at each connection seems to be adequate. Next the liquid nitrogen reservoirs are filled. The source tube and skimmer heaters are turned on and allowed to stabilize. The beam chopper is turned on and the gating circuitry checked. Often either electronic noise from the pulse amplifier or the calibrated output from the oscilloscope is counted to check the balance of the gating signals. There is ample time for these tasks due to the slow cooling of the main chamber cold shield. Even though liquid nitrogen is forced directly through the transfer lines to shorten the cooling time, three hours elapse before the entire surface approaches liquid nitrogen temperature. At this temperature the thermocouple attached to the cold shield reads 6.0 mV. It is common practice to have six 160 liter tanks of liquid nitrogen on hand the day of an experiment. At least four of them are used.

As soon as possible the beam source reservoirs are installed and degassed as follows. The contents of the ampule are frozen with liquid nitrogen and the ampule is evacuated. The ampule is then valved off and the contents warmed up to room temperature. This cycle is repeated until only a small amount of gas is liberated. This process was most important for the halogens which were

transported from the fume hood to the apparatus. Since the organometallic chemicals are never exposed to the atmosphere the degassing procedure serves only to check whether or not air has leaked into the ampule. The metal cylinders never release more than a tiny amount of gas in the first cycle, and this may well be primarily uncondensed organometallic.

About an hour before the liquid helium reservoirs are filled, they are pre-cooled with liquid nitrogen. Usually 2-3 twenty-five liter tanks of liquid helium are used during an experiment. Approximately 33 liters are needed to fill the four reservoirs initially and 20-25 liters to refill them. The main chamber dewars should retain a charge of helium for 8-10 hours. Faster boil-off is an indication of a heat leak, probably in the liquid nitrogen cooled chevron baffle which surrounds the helium reservoir. The detector helium cryopumps do not have cryogenic baffles and have to be refilled every $3\frac{1}{2}$ - 4 hours. The pressure in the main chamber ion gauge typically falls to the bottom of the 10^{-8} torr scale when helium is added; the current drawn by both ion pumps is of the order of 1 μ amp, and a large share of that is probably due to an electrical leak in one pump.

After the helium is transferred, the beam sources are turned on, optimized, and monitored for a few minutes. Only after everything is seen to perform well is the detector isolation valve opened and an angular scan begun.

An angular scan consists of two measurements at each angular point. For each measurement the radical beam is modulated at 100 Hz. One measurement of the alkyl halide signal is taken with the halogen beam intersecting the radical beam (this signal we denote S_{ON}). The other is taken with the halogen beam blocked in the source differential pumping chamber with a beam

flag (this is S_{OFF}). If the alkyl halide background had a constant D.C. level, S_{OFF} would be statistically zero; however, modulating the alkyl beam always modulates the alkyl halide background even in the absence of the halogen beam. This spurious signal seems to be related to the fact that the modulated alkyl beam is not pumped very well compared to species which condense on liquid nitrogen cooled surfaces. A diagnostic experiment aided us in deciding that the true reactively scattered signal is given by $S = S_{\text{ON}} - S_{\text{OFF}}$. For this experiment a methane beam is used in place of the alkyl radical beam. This is crossed with a chlorine beam, and the angular distribution of the mass 50 signal (same as CH_3Cl^+) is measured both with the chlorine beam on (S_{ON}) and off (S_{OFF}). Of course in this system any mass 50 signal cannot come from reaction and is probably due to space charge effects in the ionizer. The signal peaks sharply around the methane beam and gives small signals out to wide angles. The interesting point for our purposes is that $S = S_{\text{ON}} - S_{\text{OFF}}$ is statistically zero everywhere; the presence of the unmodulated halogen beam has no effect on the modulated signal. This was even true close to the direction of the chlorine beam. If the modulated background observed in the reactive scattering experiments is of identical origin, then S will indicate the true reactively scattered signal. This is an assumption implicit in the experiments. The possibility of a spurious signal present only when both beams are on is not eliminated, but we see no evidence for this. Although not necessarily so, such a signal would probably have its greatest values near one of the beams and most likely be symmetric around the beam direction. Spurious signals of this nature have been observed in the D atom, halogen reactions (MCD 72).

For all the reactions reported here S_{OFF} is typically 10-50% of S_{ON} except

when measuring close to the alkyl radical beam, in which case both S_{ON} and S_{OFF} are very large and S is zero within statistical errors. S_{ON} and S_{OFF} are accumulated in consecutive counting periods of 100 sec. at each angle. A complete angular scan can be taken in approximately $1\frac{1}{2}$ hours. In general, long counting times on each angular scan are avoided in favor of short counting times and repeated angular scans in different directions. This procedure helps to eliminate errors from sources such as long term drift of the beams.

The beam intensities are monitored very closely during an angular scan. The halogen beam intensity is checked directly with the beam monitor after every 2-3 points. An accurate method of monitoring the alkyl radical beam is to watch the source tube pressure and the pressure of ambient gas in the source chamber simultaneously. As long as the ratio of these two pressures remained constant, the beam intensity would not vary. A change in the ratio is an indication of clogging or a pumping problem, both of which affected the beam intensity. All the data shown here were taken under very steady beam conditions, with at most a few percent drift over the duration of one scan. An excellent indication of this is that the reactive signals measured on various scans at the same angle were usually within the limits set by the statistical noise expected in counting experiments.

E. Measurements

The angular distribution measurements are shown in Fig. 11. A listing of the experiments from which these curves result and a presentation of typical numbers from each experiment are given in Table II. The first thing

Figure 11
Laboratory Angular Distributions of Alkyl
Halide Reaction Products

E_{rel} is the relative kinetic energy calculated from the velocities given in Table III. Error bars indicate two-thirds confidence limits. Solid lines are drawn free hand through the points.

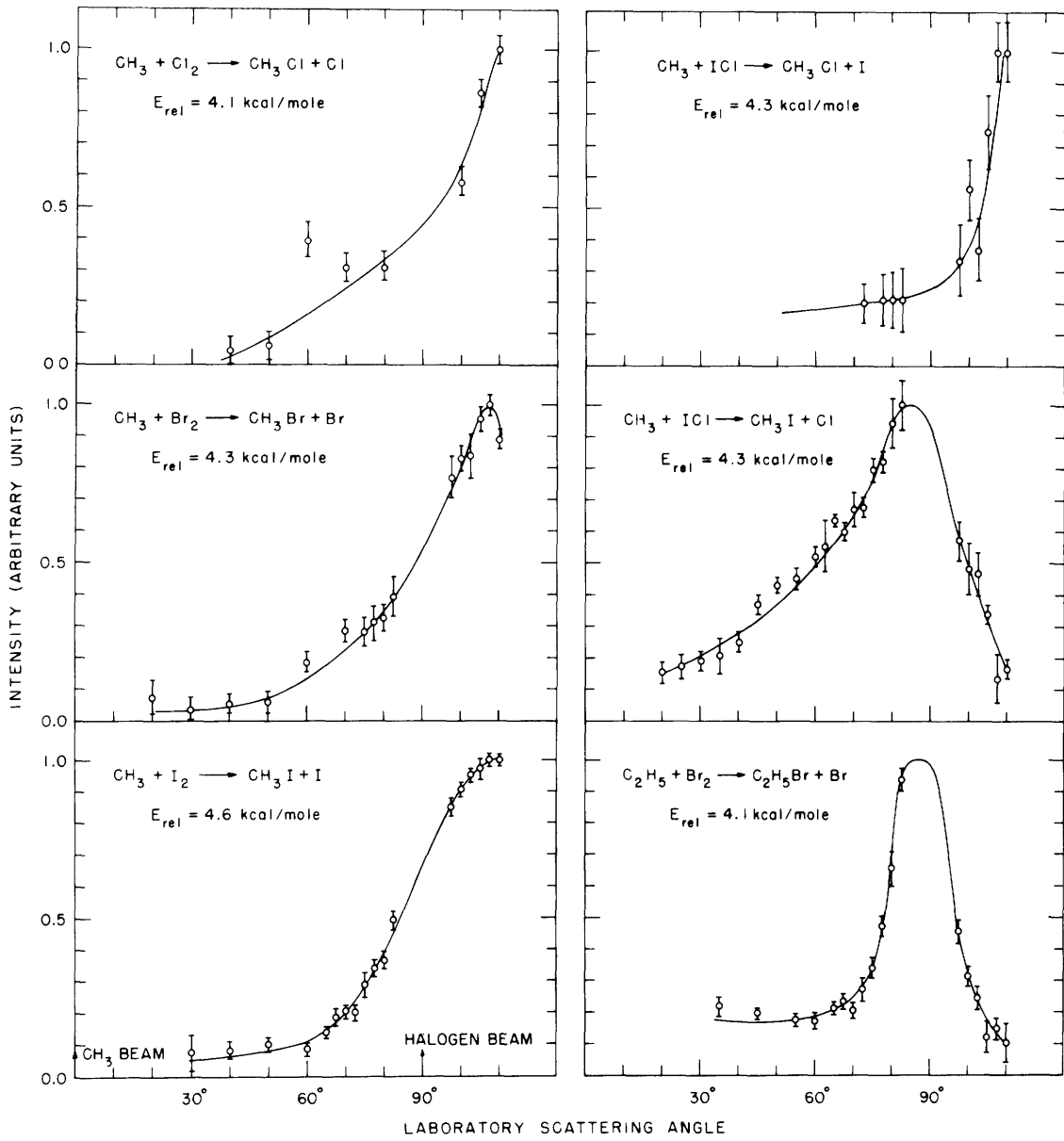


Table II

Representative Experimental Results from the
Peaks of the Angular Distribution Measurements

Total average count rate is the average number of ions per second reaching the electron multiplier. RX signal count rate is the difference per second between the signal channel and the background channel.

Reaction Product Halogen Reactant	Date	Peak Signal Levels (counts/sec)				# Angular Scans	Total Counting Time per Angle (seconds)	Signal to Noise Ratio
		Total Average Count Rate		RX Signal Count Rate				
		Halogen Beam		Halogen Beam				
		ON	OFF	ON	OFF			
$\text{CH}_3\text{Br}/\text{Br}_2$	3/14/72	900	600	100	10	5	1000	26
$\text{CH}_3\text{Cl}/\text{Cl}_2$	3/18/72	200	150	50	18	2	400	13
$\text{CH}_3\text{Br}/\text{Br}_2$	3/30/72	600	460	86	14	2	400	22
$\text{CH}_3\text{Cl}/\text{Cl}_2$	4/3/72	240	150	36	8	3	600	12
$\text{CH}_3\text{Cl}/\text{Cl}_2$	4/5/72	670	580	30	10	5	2000	12
$\text{C}_2\text{H}_5\text{Br}/\text{Br}_2$	4/21/72	560	300	103	38	4	800	22
$\text{CH}_3\text{I}, \text{I}_2$	4/24/72	825	500	198	10	4	800	33
$\text{CH}_3\text{I}, \text{ICl}$	5/10/72	4000	2900	343	25	3	600	14
$\text{CH}_3\text{Cl}, \text{ICl}$	5/18/72	160	130	23	7	3	1200	10

to notice in Fig. 11 is that the peak of the angular distribution for every system falls fairly close to the halogen beam direction. At best this is a hindrance. The problem of spurious signals is usually most severe close to an intense primary beam. We take comfort in the fact that the curves rise or fall smoothly as they pass through the region of the beam (measurements are not made $\pm 7^\circ$ from 90°) and that they are not symmetrically distributed around the beam. Furthermore, different reactions involving the same halogen beam yield satisfyingly different angular distributions. The validity of the data of course is also supported by more detailed experimental evidence. We are reasonably certain that the mass calibration of the quadrupole is very accurate. For each system the quadrupole was calibrated against the prominent isotope doublet of either chlorine or bromine. These species have high background levels and are easy to locate in the spectrum. In addition to finding signal at the expected mass, the signals disappear as the mass spectrometer is tuned slightly above and below the alkyl halide peak. What are the possible sources of spurious signal? Even though the radical source is operated at almost complete dissociation of the organometallic parent compound, the possibility exists for reactions between the parent compound and halogen molecules to give alkyl halides. However, reducing the temperature of the oven below that necessary for dissociation also causes the signal to disappear. The possibility still exists of a small amount of vibrationally excited R_2M or RM reacting with X_2 to give RX . This is ruled out on the grounds that two different parent compounds ($(CH_3)_2Zn$ and $(CH_3)_2Cd$) give the same angular distribution for CH_3Cl from CH_3 and Cl_2 despite the mass difference of 47 in the parent compounds. A final point in favor of the validity of the data is found in comparing these results with the angular distributions of DX products from

D atom, halogen molecule reactions (MCD 72). The distributions are qualitatively similar and roughly speaking the same trends are observed. Perhaps similarities in the dynamics of these two classes of reactions should not be unexpected.

Despite the points which have been made, the possibility of a systematic error in the measurements exists. Since these data represent the first reactive scattering experiments to be carried out on the apparatus described in Part I, an absolute assessment of the performance of the apparatus must be postponed until either (i) a "known" reactive angular distribution is measured or (ii) other workers confirm the results presented here.

An unusual feature of the data is the narrowness of the angular distribution for reactively scattered C_2H_5Br , the only ethyl radical reaction studied. The full width at half maximum (FWHM) is at most 40° in the center of mass (c.m.) coordinate system. The only other system for which the full width of the distribution is measured is CH_3I from ICL. The FWHM for this distribution is approximately 80° in the center of mass system. The C_2H_5Br curve shown in Fig. 11 was the result of one run, but two other runs on different days gave the same angular distribution only with lower signal to noise. An attempt was made to confirm the results by running a series of ethyl radical reactions. Electrical breakdown in the quadrupole (see Section I-E. 4) prevented running the $C_2H_5 + I_2$ reaction. The quadrupole could not be tuned up high enough to mass select C_2H_5I without the presence of huge background levels. An attempt to run $C_2H_5 + Cl_2$ was unsuccessful largely because of the inability to look directly at the mass of the reaction product. $(C_2H_5)_2Zn$ is the only ethyl-containing organometallic which was easily obtainable commercially and consequently all that we had. Unfortunately the two most prominent isotopes of Zn (mass 64 and 66) have correspondingly iden-

tical masses to the two isotopes of C_2H_5Cl (29 + 35, 37). Elastic scattering of Zn completely obscures the reactive C_2H_5Cl signal. We hoped to see a signal from the mass 49 fragment ($ClCH_2$) which is a factor of 4 smaller than the parent mass 64 peak, but this proved to be just barely possible. Small signals were observed but not of sufficient magnitude to give angular distribution measurements.

F. Features of the Angular Distributions

A number of observations can be made from the curves in Fig. 11. As we shall see for every system studied, the alkyl halide products are scattered predominantly backward in the c.m. system with respect to the incoming radical. Roughly speaking 70° in the lab. system corresponds to 90° c.m. for all these systems, and a quick glance at Fig. 11 shows that only the $CH_3 + ICl \rightarrow CH_3I + Cl$ reaction gives an appreciable amount of scattering in the forward direction.

A transformation of the laboratory measurements to the center of mass was performed assuming a nominal Newton diagram. A Focal program is based on the method presented in (HEL 68), and the calculations are performed on the Digital Equipment Corporation PDP-8/L computer attached to the apparatus. The kinematics of these reactions, especially the CH_3 , are so favorable that this nominal transformation gives a reasonably accurate picture of the c.m. distribution. The most probable Maxwellian beam velocity at $1,500^\circ K$ is chosen for the nominal alkyl radical velocity. Because of the relatively small mass of the methyl radicals (and to a lesser extent ethyl), the large spread in CH_3 velocities is not reflected in the distribution of centroids.

The halogen beam velocity, which has a much greater effect on the distribution of centroids, is expected to have a very narrow distribution (see Section II-B). The nominal velocity calculated assuming isentropic flow from the nozzle is expected to be accurate within a few percent. Also the large increase in reduced mass in these reactions causes the methyl halide product to leave the center of mass with considerable velocity. This reduces the effect of the spread of centroid velocities on the c.m. angular distributions.

With the exception of CH_3I from ICl the minimum possible speed with which the alkyl halide can leave the center of mass point is still greater than the speed of the center of mass itself. Therefore only one branch of the c.m. angular distribution contributes to the laboratory distribution. For CH_3I from ICl an iterative procedure is used to separate the relative contributions of the two branches. A zeroth order differential cross section is calculated from the angular distribution assuming that only the "fast" branch of the c.m. distribution contributes to the cross section. ("Fast" refers to the branch with higher laboratory velocity.) The equation relating the laboratory intensity and the differential cross section is:

$$I(\theta) = \frac{\sigma_{\text{FAST}}^{(0)}(\theta)}{J_{\text{FAST}}(\theta)}$$

where $I(\theta)$ is the measured lab. intensity, $J_{\text{FAST}}(\theta)$ is the transformation Jacobian for the "fast" branch, and $\sigma_{\text{FAST}}^{(0)}(\theta)$ is the zeroth order cross section mentioned above. The Jacobian includes the velocity factor which relates I to the product flux. This cross section is used as a first approximation (zeroth order) to the cross section for the "slow" branch. Now the "slow" branch can be included in a re-calculation of σ_{FAST} . To first order:

$$I(\theta) = \frac{\sigma_{\text{FAST}}^{(1)}}{J_{\text{FAST}}} + \frac{\sigma_{\text{SLOW}}^{(0)}}{J_{\text{SLOW}}} \quad \text{or} \quad \sigma_{\text{FAST}}^{(1)} = \sigma_{\text{FAST}}^{(0)} - \frac{J_{\text{FAST}}}{J_{\text{SLOW}}} \sigma_{\text{SLOW}}^{(0)}$$

The general equation for the n^{th} approximation is:

$$\sigma_{\text{FAST}}^{(n)} = \sigma_{\text{FAST}}^{(0)} - \frac{J_{\text{FAST}}}{J_{\text{SLOW}}} \sigma_{\text{SLOW}}^{(n-1)}$$

For the reaction $\text{CH}_3 + \text{ICl} \rightarrow \text{CH}_3\text{I} + \text{Cl}$ this method converges on a differential cross section, σ_{FAST} , which is somewhat smaller than $\sigma_{\text{FAST}}^{(0)}$ but has essentially identical shape.

The results of the coordinate transformation are summarized in Table III. The center of mass angular distributions are not plotted because the Jacobian factors vary so slowly that the c.m. curves differ only slightly from the lab. curves of Fig. 11. The transformation broadens the distributions somewhat, but the relevant features of the lab. distributions are retained. The c.m. angles corresponding to these features in the various distributions are found in Table III. The exact location of the peak of the c.m. distribution depends on the change in kinetic energy during the reaction (Q), which in general cannot be determined without product velocity analysis. If none of the energy released during the reaction goes into relative translational energy of the products, then $Q = 0$. The upper limit on Q is set by the reaction exoergicity which is calculated from bond energy data (VED 66). Although negative Q values are possible, they are not considered here. Table III gives the Q dependence of the peak location. The last two systems entered in the table show how little the peak position varies as a function of methyl velocity. This underscores the favorable kinematic factors of these reactions as discussed above.

Unfortunately, a large portion of almost every c.m. angular distribution

Table III

Results of lab \rightarrow c.m. Transformation

Assuming a Nominal Newton Diagram

R \cdot Vel. is the most probable alkyl radical velocity calculated assuming a Maxwellian velocity distribution at 1500 $^{\circ}$ K. X $_2$ Vel. is the most probable halogen molecule velocity calculated assuming isentropic nozzle flow (see Section II-B.). E $_{rel}$ is the relative kinetic energy calculated from these velocities.

$$Q = E_{rel}^{FINAL} - E_{rel}^{INITIAL}$$

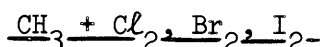
The positive value of Q is equal in each case to the reaction exothermicity calculated from bond energy data (VED 66). Max. Angle Measured corresponds to lab angle 110 $^{\circ}$, beyond which the detector cannot be rotated.

Rxn. Product Halogen Reactant	E _{rel} kcal/mole	Alkyl Vel. Halogen Vel. meters/sec	Q kcal/mole	Peak of Ang. Dist. degrees c.m.	Max. Angle measured degrees c.m.	FWHM degrees c.m.
CH ₃ Cl/Cl ₂	4.1	1580/516	0	178	178	78
CH ₃ Br/Br ₂	4.3	1580/344	20	146	146	78
CH ₃ I/I ₂	4.6	1580/300	0	153	157	38
CH ₃ Cl/ICl	4.3	1580/354	17	132	135	27
CH ₃ I/ICl	4.3	1580/354	0	152	152	
C ₂ H ₅ Br/Br ₂	4.1	1135/344	31	134	134	
CH ₃ I/I ₂	4.6	1100/300	0	142	142	
CH ₃ Cl/Cl ₂	4.1	1742/516	3	129	129	
		2500/300	0	119	180	
		1100/300	3	113	180	
		2500/300	0	130	173	
		1100/516	18	115	145	
		1742/516	5	146	146	
		2500/516	5	141	141	
			5	137	137	
			7.5	159	159	
			7.5	155	155	
			7.5	152	152	

lies in a region beyond the range of our detector. Consequently little can be said about the exact locations of the c.m. peaks or the widths of the distributions. Increasing the velocity of the halogen beam by seeding a helium nozzle beam with the halogen would solve this problem. Because of the high velocity of the methyl radicals, the relative kinetic energy would not be altered significantly. Therefore the circle, centered on the tip of the centroid, which defines the region accessible to the methyl halide products would remain roughly constant in size. However the velocity of the center of mass increases considerably, and the reactive circle moves toward and into a region accessible to the detector. Reference to Newton diagrams indicates that this effect is large and becomes more favorable the heavier the halogen is. The shift in the center of mass of the system would result in contributions to the laboratory differential cross section from both branches of the c.m. distribution, but if velocity analysis of the products is incorporated, this presents no problem.

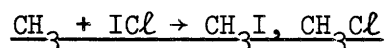
A less direct approach to the problem of shifting the center of mass is to run the reactions with CF_3 radicals instead of CH_3 . If the dynamics are similar, the center of mass shift brings the products in to smaller laboratory angles. This expectation is only one of many good reasons to study this variation of free radical reactions.

In attempting to elucidate trends in the angular distributions the systems can be grouped in various combinations.



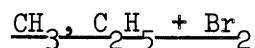
Although the peak is not established for CH_3Cl , it is evident that the distribution is narrow and that it peaks very close to 180° c.m. CH_3Br and CH_3I are shifted to smaller angles, and it appears that they peak at roughly the

same c.m. angle (~ 130 - 160° c.m.). The curves suggest that the angular distributions become broader as we go from the chloride to bromide to iodide product.



Both products are scattered backward in the c.m. system though CH_3Cl is much more sharply peaked in the backward direction. The CH_3I product is the only one measured which shows considerable scattering at less than 90° c.m.

(Remember that 90° c.m. is roughly 70° lab. angle.) In comparing the respective halide products from ICl with those from Cl_2 and I_2 we see a pronounced shift forward for CH_3I from ICl and what may be a similar shift for CH_3Cl .



The ethylbromide product peak is shifted to smaller center of mass angles, and the distribution appears to be somewhat narrower.

G. Total Reaction Cross Sections

Total reaction cross sections, Q_r , for the methyl radical reactions were calculated by Method A of (BIR 67) which is based on normalizing the reactive to the elastic scattering. The usual comparison of elastic and reactive scattering for the same system could not be made, however, because the mass 15 background from the fractionation of methane in the ionizer was too high to allow observation of elastically scattered methyl. Therefore an estimate of the relative fluxes of Zn impurity and CH_3 in the primary beam was made, and the elastic scattering of Zn from I_2 was compared with the reactive scattering of CH_3 and I_2 .

A slope of $-7/3$ was measured for the small angle differential cross section of Zn from I_2 . This is the result expected from the classical formula upon which the method is based.

The Van der Waals force constant, C , was calculated from the Slater-Kirkwood approximation with 2 and 14 effective electrons for the Zn and I_2 , respectively (HIR 54a). This assumes that the Zn $3d^{10}$ electrons are not "outer-shell" electrons. The polarizabilities used were (in \AA^3) 6.1 for Zn (LAN 50) and 9.7 for I_2 (BIR 67). The value for the polarizability of Zn given in (LAN 50) compares favorably with the value for Hg cited in (KRA 70). A calculation of Zn polarizability by the method outlined in (HIR 54b) gave a value larger by a factor of 5. The Van der Waals constant, C , was calculated to be 5.77×10^{-10} ergs \AA^6 . A most probable relative energy of 2.81×10^{-13} ergs/molecule was used. The absolute differential elastic cross section calculated from the small angle formula is:

$$\left(\frac{dQ_e}{dw}\right)_{\text{abs.}} = 99 \text{ \AA}^2/\text{str.}$$

Relative differential cross sections for elastically scattered zinc and reactively scattered CH_3I (at the peak of the reactive angular distribution) were calculated, correcting the measured intensities for: the velocity of the detected particle, the relative ionization cross sections for Zn (POT 66) and CH_3I (OTV 56), the relative primary beam intensities of Zn and CH_3 ($^{Zn}/\text{CH}_3 = 3$), the isotopic abundance of Zn (KIS 65), and the fragmentation pattern of CH_3I (ZWO 71). The ratio of these two cross sections multiplies the absolute elastic cross section to give the absolute reactive differential cross section, $\left(\frac{dQ_r}{dw}\right)_{\text{abs.}}$, which turns out to be $\sim 1 \text{ \AA}^2/\text{str.}$ for CH_3I from the $\text{CH}_3 + I_2$ reaction. A crude

integration of the c.m. angular distribution yields a value for the absolute total reaction cross section, $Q_r = 5 \text{ \AA}^2$. This calculation is accurate only to within a factor of 3 uncertainty. Interestingly enough it compares favorably with the phenomenological cross section derived from thermal rate data. Assuming that the cross section does not vary with relative kinetic energy, Q_r is given by the quotient of the rate constant and the average relative velocity, $Q_r = k/\bar{v}$. Rate data (TRO 67) for the reaction, $\text{CH}_3 + \text{I}_2 \rightarrow \text{CH}_3\text{I} + \text{I}$, studied by flash photolysis, was used to calculate a value of 3 \AA^2 for Q_r . The agreement is surprising since both methods are crude measures of the true cross section.

Based on the calculation for $\text{CH}_3 + \text{I}_2$, estimates of Q_r for methyl reacting with Br_2 , Cl_2 , and ICl are 1.5 \AA^2 for the CH_3Br product and 0.35 \AA^2 for CH_3Cl . No cross section calculation was made for the reaction, $\text{C}_2\text{H}_5 + \text{Br}_2 \rightarrow \text{C}_2\text{H}_5\text{Br} + \text{Br}$, because no attempt was made to estimate the relative ethyl flux. Since the ethyl source was operated under conditions similar to the methyl source, we might expect the radical fluxes to be the same. If this is true, then the methyl reaction with Br_2 is favored over the ethyl. Intuitively this is expected.

H. Discussion

The major contribution of the work presented here lies in the demonstration of the capability of studying polyatomic free radical reactions in beams. While we would like to be able to interpret the results in terms of the dynamics of the reactions, lack of knowledge of the product velocity distributions severely limits the conclusions which may be drawn from these

measurements. Without velocity analysis, the exact position of the peak of the c.m. angular distribution cannot be located and no information concerning the final energy partitioning in the reaction can be obtained. The size of the reactive cross sections and the marked backward peaking in the c.m. system indicate, however, that the dynamics are dominated by short range repulsion in collisions with small impact parameters.

Guided throughout the course of this work by the intuitive notion that methyl radical reactions might be dynamically similar to those of hydrogen atoms, we were particularly interested in the work of Herschbach's group at Harvard on D atom, halogen molecule reactions (MCD 72). Indeed, the similarities in the angular distributions for D and CH_3 reacting with halogens are striking. Both trends observed in the angular distributions of DX products are carried over to the CH_3X distributions.

(1) The form of the c.m. angular distribution of DX products depends primarily on the atom transferred, the peak of the distribution shifting to smaller angles as the transferred atom changes from Cl to Br to I. Roughly speaking we observe the same trend. The CH_3Cl products from Cl_2 and ICl recoil sharply into the backward hemisphere, peaking nominally beyond 150° . The CH_3Br from the Br_2 reaction is peaked less strongly backward at $\sim 130-150^\circ$. The CH_3I distribution from the I_2 and ICl reactions is quite similar to that of CH_3Br , peaking at $\sim 120-150^\circ$.

(2) The DX angular distributions show a secondary variation with the atom released. The DX products are shifted forward, by $\sim 10-20^\circ$ near the peaks, when the transferred atom is I and the released atom changes from I to Br to Cl. We observe a similar shift of $\sim 20-30^\circ$ for CH_3I from I_2 and ICl and possibly for CH_3Cl from Cl_2 and ICl .

The one distinguishing difference between the DX and CH_3X angular distributions is the amount of scattering observed in the forward hemisphere. All DX distributions show considerable scattering in the forward direction, while for CH_3X this is true only for CH_3I from ICl .

The Harvard group interpreted the product angular distributions of DX in terms of a model which states that "when the momentum arising from exit repulsion between the heavy atoms is large and impulsive, their trajectories are perturbed only slightly by the light hydrogen atom. The direction of recoil therefore corresponds approximately to the angle between the axis of the target molecule and the initial relative velocity vector at the onset of the X-Y repulsion." The validity of this interpretation depends both on the light mass of the D atom and on the knowledge of the final relative kinetic energy of the products. In our experiments the CH_3 radical carries in roughly twice the momentum carried by the D atom. The exothermicities of the CH_3 , halogen molecule reactions are only about half as large as those of the D, halogen reactions, so that even if the same fraction of energy is channeled into translation, the perturbation caused by the CH_3 is a factor of 3 larger than that caused by the D atom. Without velocity analysis of the CH_3X products, however, an assessment of the applicability of the model cannot be made. Perhaps the lack of complete agreement in the observed trends is related to a breakdown in the model.

The internal degrees of freedom of CH_3 are expected to have only a small effect on the dynamics of these reactions. As the reaction proceeds, the structure of the radical changes from planar to tetrahedral. The energy required to bend the methyl to the tetrahedral configuration is estimated to be less than ~ 6 kcal/mole, which represents the barrier to inversion in

NH_3 . CH_3 bending is expected to require a smaller amount of energy since CH_3 has one less electron than NH_3 . The energy can easily be supplied by the formation of the C-X bond, in which case we might expect a smaller fraction of the total available energy to end up in translation of the products for the CH_3 reactions as compared to the D atom reactions. The energy could also be supplied by internal excitation of the CH_3 radicals in the beam. However, we have no information concerning the internal state distribution of CH_3 , due to the non-equilibrium behavior of the pyrolysis source.

Experiments in which methyl-halogen bonds are broken also provide evidence that there is relatively little energy associated with the puckered configuration of CH_3 . The following examples demonstrate that the CH_3 relaxes to the planar structure in such a way that the energy released into vibration as the bond is broken is small.

(1) A molecular beam study of the reaction, $\text{K} + \text{CH}_3\text{I} \rightarrow \text{KI} + \text{CH}_3$, has been performed with velocity analysis of the products (RUL 72). About 40% of the total available energy is partitioned among internal degrees of freedom in the products. There is some evidence based on the residual detection of KI in the non-detecting mode that the KI is highly vibrationally excited; and thus, by difference, the CH_3 is internally "cold".

(2) Unpublished molecular beam results comparing the velocity spectra of KI from the reactions, $\text{K} + \text{CH}_3\text{I}$ and $\text{K} + \text{CF}_3\text{I}$, show indirectly that after reaction CH_3 is no more internally excited than CF_3 is, even though CF_3 (pyramidal) and CH_3 (planar) differ in structure (HER 72).

(3) The photodissociation translational spectrum of CH_3I also indicates that methyl relaxes adiabatically as the C-I bond is cleaved (RIL 72). The

photodissociation of CH_3I into CH_3 and ground state I involves the partitioning of roughly 60 kcal/mole of energy, of which less than 15% was found as internal energy of the CH_3 radical.

We have no information concerning the final energy partitioning in these reactions. Work has been started on the addition of a time-of-flight velocity analyzer to the apparatus described in Part I. In the near future, results of chemiluminescence experiments involving the reactions, $\text{CH}_3 + \text{F}_2$ and $\text{CH}_3 + \text{Cl}_2$, will give direct measurements of the energy partitioning (MCD 72B).

References

- ASH 66 H. Ashkenas and F. S. Sherman, in J. H. deLeeuw, ed., Rarefied Gas Dynamics (4th Symposium) (1966).
- BEC 68 D. Beck, F. Engelke, and H. J. Loesch, Ber. Bunsenges Physik. Chem. 72, 1105 (1968); Cl + Br₂.
- BIC 70 R. W. Bickes, Jr. and R. B. Bernstein, Rev. Sci. Instrum. 41, 759 (1970).
- BIR 67 J. H. Birely, R. R. Herm, K. R. Wilson, and D. R. Herschbach, J. Chem. Phys. 47, 993 (1967).
- BIR 69 J. H. Birely, E. A. Entemann, R. R. Herm, and K. R. Wilson, J. Chem. Phys. 51, 5461 (1969).
- BRI 67 G. O. Brink, Rev. Sci. Instrum. 37, 857 (1966).
- BUR 67 C. N. Burrous, A. J. Lieber, and V. T. Zaviantseff, Rev. Sci. Instrum. 38, 1477 (1967).
- COR 42 J. Cornog and E. E. Bauer, J. Am. Chem. Soc. 64, 2620 (1942).
- CRO 69 J. B. Cross and N. C. Blais, J. Chem. Phys. 50, 4108 (1969); Cl + Br₂.
- CRO 70 N. C. Blais and J. B. Cross, J. Chem. Phys. 52, 3580 (1970); Cl + Br₂; J. Chem. Phys. 55, 3970 (1971); Cl + I₂, IBr.
- DAT 63 S. Datz and E. H. Taylor, J. Chem. Phys. 39, 1896 (1963).
- DAT 67 S. Datz and T. W. Schmidt, Proceedings of the Fifth International Conference on the Physics of Electronic and Atomic Collisions (Publishing House Navka, Leningrad, 1967).

- EGI 69 A. Edidi, R. Marconero, G. Pizzella, and F. Sperli, Rev. Sci. Instrum. 40, 88 (1969).
- FIT 63 W. L. Fite and R. T. Brackmann, in Atomic Collision Processes, M. R. C. McDowell, Ed. (North Holland Publishing Co., Amsterdam, 1963), p. 955.
- FIT 65 W. L. Fite and R. T. Brackmann, J. Chem. Phys. 42, 4057 (1965).
- GED 70 J. Geddes, H. F. Krause, and W. L. Fite, J. Chem. Phys. 52, 3296 (1970); D + H₂.
- GEN 67 W. R. Gentry, U. C. Berkeley Lawrence Radiation Lab. Report, UCRL - 17691.
- GOR 71 R. J. Gordon, Y. T. Lee, and D. R. Herschbach, J. Chem. Phys. 54, 2393 (1971).
- GOU 66 F. S. Goulding, Nuclear Inst. and Methods 43, 1-54 (1966).
- HEL 68 R. K. B. Helbing, J. Chem. Phys. 48, 472 (1968); erratum: 50, 4123 (1969).
- HER 72 D. R. Herschbach, private communication.
- HIR 54a J. O. Hirschfelder, C. F. Curtiss, and R. B. Bird, Molecular Theory of Gases and Liquids (John Wiley & Sons, New York, 1954) p. 964.
- HIR 54b Ibid., pp. 952-954.
- HIR 54c Ibid., p. 950.

- HON 60 R. E. Honig and H. O. Hook, RCA Review, 21, 360 (1960).
- KAL 69 F. Kalos and A. E. Grosser, Rev. Sci. Instrum. 40, 804 (1969).
- KIN 72 J. L. Kinsey, MTP International Review of Science, Physical Chemistry Series One: Vol. 9, Chemical Kinetics (J. C. Polanyi, Ed.), Chapter 6: Molecular Beam Kinetics.
- KIS 65 R. W. Kiser, Introduction to Mass Spectrometry and Its Applications, Appendix A (Prentice-Hall, New Jersey, 1965).
- KRA 70 H. L. Kramer and D. R. Herschbach, J. Chem. Phys. 53, 2792 (1970).
- LAM 57 F. W. Lampe, F. H. Field, and J. L. Franklin, J. Am. Chem. Soc. 79, 6129 (1957).
- LAN 50 Landolt-Börnstein, Zahlenwerte und Funktionen, I Band, "Atom - und Molekular Physik", I Teil, Atome - Ionen, (Springer-Verlag, 1950), pp. 399-401.
- LEE 68 Y. T. Lee, J. D. McDonald, P. R. LeBreton, and D. R. Herschbach, J. Chem. Phys. 49, 2447 (1968); $Cl + Br_2$, $Br + I_2$.
- LEE 69 Y. T. Lee, J. D. McDonald, P. R. LeBreton, and D. R. Herschbach, Rev. Sci. Instrum. 40, 1402 (1969).
- LEE 69b Y. T. Lee, J. D. McDonald, P. R. LeBreton, and D. R. Herschbach, J. Chem. Phys. 51, 455 (1969); $Cl + IBr$, $Br + ICl$.
- MAS 64 E. A. Mason, J. T. Vanderslice, and C. J. G. Raw, J. Chem. Phys. 40, 2153 (1964).

- MCD 63 C. A. McDowell, Ed., Mass Spectrometry, pp. 210-221 (McGraw-Hill Book Co., New York, 1963).
- MCD 63b Ibid., Chapter 11.
- MCD 72 J. D. McDonald, P. R. LeBreton, Y. T. Lee, and D. R. Herschbach, *J. Chem. Phys.* 56, 769 (1972).
- MCD 72b J. D. McDonald (U. of Illinois), private communication.
- MCF 72 D. L. McFadden, E. A. McCullough, Jr., F. Kalos, W. R. Gentry, and J. Ross, *J. Chem. Phys.* 57, 1351 (1972).
- OTV 56 J. W. Otvos and D. P. Stevenson, *J. Am. Chem. Soc.* 78, 546 (1956).
- OWE 48 P. L. Owen and C. K. Thornhill, Aeronautical Research Council (U.K.) R + M, No. 2616 (1948).
- PAN 29 F. A. Paneth and W. Hofeditz, *Ber.*, 62B, 1335 (1929).
- PAO 67 F. R. Paolini and G. C. Theodoridis, *Rev. Sci. Instrum.* 38, 579 (1967).
- PAU 53 W. Paul and H. Steinwedel, *Z. Naturforsch.*, 8a, 448 (1953).
- PAU 55 W. Paul and M. Raether, *Z. Physik*, 140, 262 (1955).
- PAU 58 W. Paul, H. P. Reinhard, and U. von Zahn, *Z. Physik*, 152, 143 (1958).
- POT 66 R. F. Pottie, *J. Chem. Phys.* 44, 916 (1966).
- PUR 38 E. M. Purcell, *Physical Review*, 54, pp. 818-826 (1938).

- RIL 72 S. J. Riley, (U. C. La Jolla), private communication.
- RUL 72 A. M. Rulis, Ph.D. Thesis (U. of Wisconsin, 1972) WIS-TC1-476X.
- SEP 67 Albert Septier, Ed., Focusing of Charged Particles, Vol. 1, Chapter 2.2, "Electrostatic Lenses", (Academic Press, New York, 1967).
- SPA 48 K. R. Spangenberg, Vacuum Tubes, Chapter 13, "Electrostatic Electron Optics", (McGraw-Hill, New York, 1948).
- TRO 67 A. F. Trotman-Dickenson and G. S. Milne, Tables of Bimolecular Gas Reactions (NSRDS-NBS 9, 1967), p. 51.
- VED 66 V. I. Vedeneyev, L. V. Gurvich, V. N. Kondrat'yev, V. A. Medvedev, and Ye. L. Frankevich, Bond Energies, Ionization Potentials and Electron Affinities (E. Arnold, London, 1966).
- WOO 20 R. W. Wood, Proc. Roy. Soc. (London), A97, 455 (1920).
- WOO 21 R. W. Wood, Phil. Mag. 42, 729 (1921).
- WOO 22 R. W. Wood, Proc. Roy. Soc. (London), A102, 1 (1922).
- WOO 22b R. W. Wood, Phil. Mag. 44, 538 (1922).
- ZWO 71 B. J. Zwolinski, Director, American Petroleum Institute Research Project 44, "Selected Mass Spectral Data", 1971.

APPENDIX A

Currently Available Mechanical DrawingsA seriesVacuum system

1. Main vacuum chamber
2. Vacuum chamber stand
3. Cryopump chamber
4. Source chamber
5. Side flange
6. Main chamber blank-off flange
7. Pressure release flange
8. Cold shield
9. Cold shield side plate
10. Cold shield extension
11. Cold shield support screw
12. Liquid nitrogen feed tube
13. Cryopump heat shield
14. Diffusion pump spool
15. Source differential pump chamber (obsolete)
- 15M. Source differential pumping chamber modification
- 15a. Source differential pumping chamber bulkhead front plate
- 15b. Source differential pumping chamber copper cold shield
- 15c. Source differential pumping chamber adjustable aperture
16. Main chamber rotating lid
17. Diffusion pump spool blank-off flange
18. Detector differential pumping chamber
19. Detector chamber back flange
20. Aperture retaining ring
21. Aperture
22. Rotating lid driven gear
23. Radiofrequency feedthrough flange
24. Quadrupole mass filter end plate modification
25. Liquid helium cryopump

- 25a. Plug for helium cryopump
26. Ion counter coupling chamber
27. Rotating lid drive gear
28. Drive gear bearing
29. Platform frame
30. Side flange copper gasket
31. Source chamber clank-off flange
32. Rotating lid installation bracket
33. Ionizer and lens mount plate
36. Detector window retainer
37. Detector window
38. Retainer installation tool
39. Rotating lid center flange
40. Rotating lid flange A
41. Rotating lid flange B
42. Rotating lid vernier
43. Vernier holder
44. Source chamber trap
45. Source chamber liquid nitrogen feedthrough
46. Cryopump radiation shield

B series Beam Sources

1. Beam source assembly (obsolete)
2. Oven support and gas handling (obsolete)
3. Mounting flange (obsolete)
4. Pump-out port flange (obsolete)
5. Source tube (obsolete)
6. Multichannel aperture
7. Source nut
8. Nozzle aperture
9. Methyl beam source tube (2 drawings)
10. Methyl beam source aperture
11. Permanent gas beam source (2 drawings)

12. Permanent gas beam source aperture
13. Source tube collar
14. Blank-off flange for source flange ports
15. Source chamber flange (2 drawings)
16. Source tube compression seal feedthrough
17. Ampule smasher
18. Source chamber front plate
19. Skimmer mount

I series Ionizer

1. Ionizer support stand
2. Einzel lens plates No. 2 and No. 3
3. Einzel lens plates No. 2
4. Extracting grid plate No. 4
5. Extracting grid plate No. 5
6. Entrance aperture plate No. 6
7. Ionizer shield spool
8. Filament support
9. Filament support insulators
10. Ionizer support screw insulators
11. Ionizer support rod spacer
12. Ionizer support rods
13. Ionizer assembly
14. Ionizer einzel lens, spherical lens schematic circuit design
15. Filament holder insulator

N series Spherical Lens

1. Support block
2. Concave element
3. Convex element
4. Assembly

P series Ion Counter

1. Cylindrical lens support rod
2. Cylindrical lens element No. 1
3. Cylindrical lens element No. 2, 3, and 4
4. Cylindrical lens element No. 5
5. Cylindrical lens top support
6. Vacuum chamber
7. High voltage feedthrough flange
8. Liquid N₂ feedthrough flange and reservoir
9. Semiconductor mount
10. Semiconductor retainer
11. Semiconductor mount high voltage shield
12. High voltage terminal fitting
13. Anti-corona ball
14. High voltage shield
15. High voltage shield end window
16. Faraday cup
17. Faraday cup shield
18. Cylindrical lens spacers

Z series Test Stand

1. Base plate
2. Blank-off flange
3. Plexiglass blank-off flange
4. Main chamber
5. Connecting spool flange
6. Connecting spool
7. Vacuum stand
8. Ionizer test flange
9. Platform support plate
10. Feedthrough shield
11. Vacuum test stand platform
12. Ionizer test flange window

13. Feedthrough shield cover
14. Test source flange
15. Test source support
16. Test source
17. Thin aperture
18. Leak valve connector
19. Vacuum test stand and plate
20. Vacuum test stand caster blocks

M series

Miscellaneous

1. Titanium pump 12" base assembly
2. Titanium pump curvac connector 6"
3. Titanium pump 18" conc. comb. baseplate
4. 12" Vacuum chamber module
5. High Q head mounting bracket
6. Feedthrough flanges
7. Corner connector for 12" module
8. Block diagram of super machine
9. Primary beam electron bombardment monitor differential ionizer frame
10. Primary beam electron bombardment monitor differential ionizer cover
plate
11. Differential ionizer control panel
12. High voltage lens focusing potentials
13. High voltage lens switching circuit
14. Ionizer and spherical lens energy analyzer control panel
15. Quadrupole insulator

APPENDIX B

Suppliers of Commercial Items

1. Quadrupole Mass Filter
ExtraNuclear Laboratories
P.O. Box 11512, Pittsburgh
Pennsylvania 15238
(412) 828-8508
2. Pulse Counting Electronics
Canberra Industries
50 Silvera Street
Middletown, Conn. 06457
(203) 347-6995
3. Amphenol Connectors
Richard Purinton, Inc.
11 Muzzey Street
Lexington, Mass.
862-8300
4. Screws, Nuts, Washers
Industrial Stainless Steels, Inc.
Cambridge, Mass.
864-7700
5. Ion Pumps
Titanium Sublimation Pumps
Curvac Flanges
Copper Gaskets
Nude Ion Gauges
Zeolite Foreline Trap
Vac-Seal Epoxy Resin
Ultek, Div. of Perkin-Elmer
599 North Avenue, Door 8
Wakefield, Mass. 01880
6. Kepco Power Supplies
Ray Perron and Co., Inc.
159 Moore Street
Norwood, Mass. 02062
762-8114
7. Operational Amplifiers
Philbrick/Nexus Research
Allied Drive at Route 128
Dedham, Mass. 02026
329-1600
8. General Electrical Supplies
and Accessories
Cramer Electronics
320 Needham Street
Newton, Mass. 02164
969-7700

- DeMambro Electronics
1095 Commonwealth Avenue
Boston, Mass. 02215
787-1200
9. O-Ring Compression Seals
Industrial Equipment and Sales
Corporation
84 State Street
Boston, Mass.
227-0838
10. Parker O-Rings
I. B. Moore Corporation
30 Rindge Avenue, Ext.
Cambridge, Mass.
491-0100
11. Rigid Air Lines, General Radio,
BNC, UHF, Adaptors and Connectors
General Radio
22 Baker Avenue
West Concord, Mass.
646-0550
12. Power Designs Power Supplies
Power Designs, Inc.
1700 Shames Drive
Westbury, New York
13. Electronics Racks
Technical Instruments, Inc.
122 West Street
Wilmington, Mass.
14. Si(Li) Semiconductor
Kevex Corporation
898 Mahler Road
Burlingame, Calif. 94010
(415) 697-6901
15. Main Chamber H₂ Brazing
Wall Colmonoy Corporation
19345 John R Street
Detroit, Mich. 48203
(313) 893-3800
16. Insulating Foam
Plastic Packaging Materials, Inc.
2235 N. Bodine Street
Philadelphia, Pa. 19133
17. 1000 lb. Electric Hoist
Langley Handling Equipment
966 Cambridge Street
Cambridge, Mass.
395-8010

18. Tuning Fork Chopper
American Time Products
61-20 Woodside Avenue
Woodside, New York 11377
19. Teletype
Teletype Corporation
5555 Touhy Avenue
Skokie, Illinois
20. Linde Liquid N₂ Cold Trap Reservoirs
Cryogenics - East
Wheeler Road
Burlington, Mass. 01803
21. Johns Technology, Inc. Liquid
N₂ Level Control
American Dynamics Corporation
17 Dunster Street
Cambridge, Mass.
22. Custom-Made Tec Rings
Tec-Seal Corporation
P.O. Box 4646
Wilmington, Calif. 90744
23. Four Point Contact Radial Ball
Bearing
Kaydon Eng. Corp. Sales Rep.
W. A. Smith, Jr.
1004 Main Street
Hingham, Mass.
24. Metal Hose
Anaconda Metal Hose Division
824 Boylston Street
Chestnut Hill, Mass. 02167
734-8205
25. Sorenson Line Voltage Regulator
and Power Supplies, Dana
Digital Voltmeter
Instrument Associates
30 Park Avenue
Arlington, Mass. 02174
26. Drafting Table and Accessories
B. L. Makepeace, Inc.
1266 Boylston Street
Boston, Mass.
267-2700
27. Picoammeter
Keithley Instruments, Inc.
235 Bear Hill Road
Waltham, Mass.
28. John Fluke Power Supplies
Technical Instruments, Inc.
122 West Street
Wilmington, Mass.
29. Phase Shifter/Meter
Aritech Corporation
130 Lincoln Street
Boston, Mass. 02133
254-2990

30. Moseley X-Y Recorder
Hewlett-Packard, Yewell Sales
Division
Middlesex Turnpike
Burlington, Mass.
31. Vibrating Reed Electrometer
Cary Instruments
232 Washington Street
Belmont, Mass. 02178
32. Machining of Rotatable Lid
Industrial Tool and Machine Co.
Higgins Street
Georgiaville, R.I.
231-6700
33. Glass-encapsulated Resistors
B & W Associates
110 Great Road
Bedford, Mass.
34. Variable Leak Valves
Granville-Phillips Co.
5675 East Arapahoe Avenue
Boulder, Colo. 80302
35. Main Chamber Machining
Walter W. Field & Son
660 Arsenal Street
Watertown, R.I.P.
36. Alumina Insulators
McDanel Refractory Porcelain Co.
510 Ninth Avenue
Beaver Falls, Pa. 15010
37. Unislide Assembly
Tropel, Inc.
52 West Avenue
Fairport, New York 14450
38. Diffusion Pumps
Slide Valves
Ion Gauge Controls
Norton Vacuum Equipment Div.
865 Providence Highway
Dedham, Mass.
39. Digitec Digital Voltmeter
Carl Lueders & Co.
P.O. Box 161
Needham Heights, Mass.
40. Glass Capillary Fused Array
New England Technical Sales Corp.
7 Cypress Drive
Burlington, Mass.
272-0434
41. Sapphire Spheres, Insulators
Adolf Mellor Co.
P.O. Box 6001
Providence, R.I. 02904

42. High Voltage Terminal Bushing
Alite Division, U.S. Stoneware
Box 119
Orville, Ohio 44667
(216) 669-2271
43. Electroformed Mesh
Buckbee Mears Co.
245 E. 6th Street
St. Paul, Minn. 55101
44. Indium Wire, Foil and Sheets
The Indium Corp. of America
P.O. Box 269
Utica, New York 13503
(315) 797-1630
45. Liquid He Cryopumps, Helium
Transfer Tube
Janis Research Co., Inc.
22 Spencer Street
Stoneham, Mass. 02180
46. Computer PDP ⁸/L Softwares
(Modules, Cables, Wires,
Programmed Tapes, etc.)
Digital Equipment Corp.
Program Library
146 Main Street
Maynard, Mass. 01754
47. Tantalum Foil
A. D. MacKay, Inc.
198 Broadway
New York, New York 10038
(212) BA7-8730
48. Dimethylzinc, Dimethylcadmium,
Diethylzinc, etc.
Alfa Inorganics
P.O. Box 159
Beverly, Mass. 01915
49. Spiraltron Electron Multiplier,
CEM-4028 Capped Collector
Bendix Electro-Optics Div.
Sturbridge, Mass.
50. Hysteresis Synchronous Motor
Globe Industries
Division of TRW
2275 Stanley Avenue
Dayton, Ohio 45404
51. Butterfly Valve
Edwards High Vacuum, Inc.
554 Main Street
South Weymouth, Mass. 02190
52. Epoxy
Emerson & Cummings, Inc.
Canton, Mass.
828-3300

53. Nupro Metering Valves
Cajon Fittings
Swagelok Fittings
Cambridge Valve & Fitting Co.
334 Boston Post Road
Wayland, Mass.
237-0942
54. Bellows Seal Valves
Joseph Bertram & Co.
60 Dedham Avenue
Needham, Mass. 02192
55. Vacuum Valves
Goddard Valve Corporation
Worcester, Mass.
(617) 755-8635
56. Blackstone Ultrasonic Cleaner
Technical Instruments, Inc.
122 West Street
Wilmington, Mass. 01887

Biographical Sketch

David Lee McFadden was born October 18, 1945 at St. Joseph's Hospital in Orange, California. His childhood was spent in Southern California. During his last three years of high school, he lived in Phoenix, Arizona, where he was graduated in 1963 from Camelback High School. He spent four years at Occidental College in Los Angeles as an Alfred P. Sloan Foundation Scholar and was graduated cum laude in 1967 with an A.B. degree in Chemistry. He was elected to Phi Beta Kappa.

He entered M.I.T. in the Fall of 1967. During the past five years, he has held appointments as a teaching assistant, research assistant, and NSF trainee. On June 28, 1970 he married Martha Hope Fudim. He has co-authored the paper, "Molecular Beam Study of Polyatomic Free Radical Reactions". He is a member of the American Physical Society and Sigma Xi.

"The bird of Time has but a little way
To fly . . . and, lo! the bird is on the wing"